Title	Challenges in material and structure design of zinc anode toward high-performance aqueous zinc-ion batteries
Author(s)	Wencheng Du, Edison Huixiang Ang, Yang Yang, Yufei Zhang, Minghui Ye and Chengchao Li
Source	*Energy and Environmental Science,* (2020)
Published by	Royal Society of Chemistry

Energy & Environmental Science

Accepted Manuscript

This article can be cited before page numbers have been issued, to do this please use: W. Du, E. H. Ang, Y. Yang, Y. Zhang, M. Ye and C. Li, *Energy Environ. Sci.*, 2020, DOI: 10.1039/D0EE02079F.

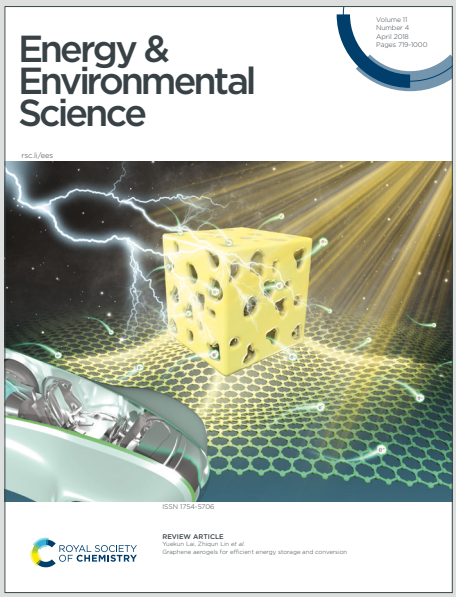

ROYAL SOCIETY OF CHEMISTRY

rsc.li/ees

View Article Online
DOI: 10.1039/D0EE02079F

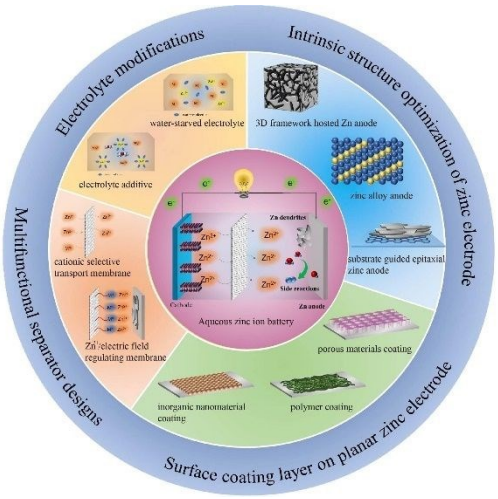

This review summarizes the recent progress in material and structural designs of zinc anode for high-performance aqueous zinc ion batteries.

View Article Online
DOI: 10.1039/D0EE02079F

Challenges in Material and Structure Design of Zinc Anode toward High-Performance Aqueous Zinc-Ion Batteries

Wencheng Du,[a] Edison Huixiang Ang,[b] Yang Yang,[a] Yufei Zhang,[a] Minghui Ye[a] and Cheng Chao Li*[a]

[a]School of Chemical Engineering and Light Industry, Guangdong University of Technology, Guangzhou 510006, China

[b]Natural Sciences and Science Education, National Institute of Education, Nanyang Technological University, 637616, Singapore

E-mail: licc@gdut.edu.cn

Keywords: aqueous zinc ion batteries, zinc anode, materials, structures

View Article Online
DOI: 10.1039/D0EE02079F

Rechargeable aqueous metal-ion batteries are very promising because of their green and safe inherent features as alternative energy storage devices during the post-lithium-ion era. Aqueous zinc ion batteries (ZIBs) have been studied extensively among different aqueous metal ion batteries recently due to some unique and outstanding benefits of ZIBs that promise for large-scale power storage systems. However, zinc anode problems in ZIBs such as zinc dendrite and side reactions severely shorten ZIB's cycle lifetime, thus restricting their practical application. Here, we sum up in detail recent progress of general strategy to suppress zinc dendrite and zinc anode side reactions based on advanced material and structure design including the modification of planar zinc electrode surface layer, internal structural optimization of zinc bulk electrode, modification of the electrolyte and construction of the multifunctional separator. The various functional materials, structures and battery efficiency are discussed. Finally, the challenges for ZIBs are identified in their production of functional zinc anodes.

1. Introduction

Rechargeable batteries are crucial to people's lives today because they not only bring great convenient service to people's work and life, they also produce a more green world as they slowly replace conventional fossil fuels that can cause significant environmental pollution.[1, 2] Owing to their high energy density and long cycle lifetime, lithium ion batteries have dominated the applications of secondary batteries in the last 30 years.[3–7] Increased energy storage technology is needed in the development of human society. Lithium ion batteries today face a variety of issues with their cores. In addition to the immediate need for a greater energy density of lithium ion batteries for high-performance electric vehicles with equal mile range to conventional vehicles powered by an internal-combustion engine. Two fatal failures are faced by lithium ion batteries. The possible safety issue limits its use in massive energy storage environments, especially of the intrinsically inflammable organic electrolyte, is so complicated to eradicate. The other problem is that there is a significant shortage of lithium supplies because of a rising demand for lithium on the earth. The problem of lithium resource deficiency will inevitably reduce its long-term use in lithium ion batteries. It is therefore necessary to search for new battery technology based on a safer battery system and other metal-based electrode materials with a higher abundance on Earth.

In order to create a better world of energy storage, researchers are devoting themselves to studying other metal-based batteries and simultaneously adopting safe aqueous electrolytes instead of organic ones. To date, numerous rechargeable aqueous metal-ion batteries have been developed and may become a dominant energy system in the future.[8–13] Among these new metal-ion batteries, including sodium, potassium, aluminum, calcium and zinc, aqueous zinc-ion batteries (ZIBs) have received considerable attention and are considered to be the most promising candidates for large-scale energy storage systems in the future due to their many intrinsic merits:[14–18] (1) Zinc is three times the number of elements of lithium. Therefore, ZIBs

View Article Online
DOI: 10.1039/D0EE02079F

have major resource advantages; (2) ZIB assembly needs no inert environment that dramatically reduces battery assembly costs; (3) Zinc metal can be used directly as anode above other metals (lithium, magnesium, calcium and aluminum). This benefits from the high stability and reversible electrodeposition of zinc in the aqueous electrolyte; (4) Zn metal as anode possess a high theoretical volumetric and gravimetric capacity of 5855 mAh cm^{-3} and 820 mAh g^{-1}, respectively, and low oxidation/reduction potential of -0.76V *vs.* standard hydrogen electrode, indicating possible high open voltage when couple with a cathode; (5) There is no environmental toxicity of zinc metal and its salts that ensures the high level of ZIB safety. Such beneficial qualities make ZIBs attractive in different ways, so that much attention has been paid in recent years.

Although aqueous zinc-based batteries like Zn-MnO_2, Zn-air and Zn-metal batteries have been researched since the 1860s[19–23] and some of which were commercialized, the commercial zinc-based energy storage systems available are predominantly primary batteries that could result in resources and environmental stress unless recovery is achieved. The transformation from primary to secondary batteries of zinc-based batteries is therefore of great importance in the effective use of energy. In the 1960s, various attempts were made to improve zinc-manganese batteries in alkali media for the production of rechargeable zinc batteries.[24, 25] However, their implementation was seriously restricted by poor cycling life and undesirable capabilities/efficiency. Between 1986-1988, Yamamoto and Shoji *et al.* reported rechargeable aqueous Zn-MnO_2 batteries with mild aqueous electrolytes such as aqueous $ZnSO_4$ electrolyte instead of common alkaline electrolyte, which opened the door for rechargeable aqueous ZIB based on near-neutral electrolytes.[26, 27] The substitution of alkaline electrolyte with neutral one can mitigate severe corrosion in ZIBs and helps to reduce the formation of electrically insulated by-products such as solid ZnO and $Zn(OH)_2$ that can passivate on the zinc anode. Since 2012, Kang's group has developed a ZIB that is based on β-MnO_2 cathode material and the 1 M $ZnSO_4$ electrolyte with obvious improvement in cycle life.[28] The fast production of different

View Article Online
DOI: 10.1039/D0EE02079F

cathode materials and mild aqueous electrolytes to increase ZIBs' rechargeability while simultaneous promotion of new science growth.

In recent years, several efforts have concentrated on developing appropriate cathode materials for increased zinc storage. A wide range of cathodic materials, including manganese oxides, vanadium oxides, and organic active molecules have been created.[29–36] The optimization of material/structure and in-depth storage mechanism analyzes for cathode material clearly improve their performance in zinc storage. However, the research on zinc anode is inadequate, and zinc anode is also critical for cycling performance of the full battery. Two problems of zinc anode, including zinc dendrite and water/oxygen-related side reactions have an impact on cycling performance.[37–48] Similar to lithium anode, the electrodeposition of zinc tends to form zinc dendrites with irregular structure.[49] The inevitable result of the dendrite growth is causing internal short-circuit faults. Furthermore, zinc possesses high mechanical strength with Young's modulus of 108 GPa, much higher than those of Li (5 GPa) and Na (10 GPa).[49] This fact means that zinc dendrites can pierce through separators easily once large-scale growth, causing failure of battery.

Besides zinc dendrite issue, water/oxygen-induced side reactions accompanying the zinc deposition/stripping process is another problem degrading the cycling performance of ZIBs.[41, 50] For example, compared with traditional aqueous alkaline electrolyte, although recently applied near-neutral electrolytes have unique merits in suppressing electrode passivation, the electrolytes provide stronger thermodynamic tendency for hydrogen evolution reactions (HER) on zinc surface because of the higher activity of proton in near-neutral electrolytes.[37, 41] So, HER may compete with the electrodeposition reaction of zinc, resulting in low Columbic efficiencies and the produced gas will cause electrolyte leaking. These undesirable results will degrade battery performance or even fail the battery. Therefore, the optimization of zinc anode by material and structural designs is very critical in order to create dendrite-free and highly stable zinc anode systems. So far, more and more strategies begin to present to improve zinc

View Article Online
DOI: 10.1039/D0EE02079F

anode based on choosing functional materials and designing the specific structures to optimize zinc anode itself and related systems such as electrolyte or separator components. Zinc electrode as one component of the battery system has connected relation with other parts including bulk electrolyte and separator. The efficiency of zinc anode can thus be improved by rational modifications of each component. Rational materials and structures of each ZIB component are essential to the optimum improvement of electrochemical performances for zinc anode system. Some efforts were made to outline the progress of zinc anode from various perspectives and focus areas,[37-48] which are helpful for solving complicated chemical/electrochemical issues of zinc anode in aqueous media. However, a comprehensive and detailed review about designing ideals and enhanced efficiencies of diverse materials/structures toward zinc anode has not been published until today.

In this context, we will systematically review the recent progress in material and structural design towards a high-performance zinc anode. First, we will provide the principles of chemical thermodynamics of the zinc electrodeposition process in order to show the microscopic reasons of zinc anode problems, which are the theoretical basis of choosing suitable materials and designing specific structures. Then, we will emphasize the various strategies to enhance zinc anode performance from various aspects including zinc electrode surface modification techniques, zinc bulk electrode structure optimization, electrolyte modifications and multifunctional separator designs. We will see that precise material and structure regulation is vital for obtaining ideal enhanced effects. These strategies provide a valuable reference for searching a more practical route to construct high-performance zinc anodes. Finally, the challenges of developing practical zinc anode with high performances are discussed. This will be helpful to understand the various zinc anode enhancement strategies, which will directly benefit the future commercialization of ZIBs.

2. Interfacial electrochemistry of zinc anode

In ZIBs, cathode reactions are different depending on different types of cathode materials. For example, typical intercalation/conversion reactions for metal oxides such as MnO_2, while red/ox reactions of active groups when organic molecules such as PANI or tetra-chloro-benzoquinone used as cathode materials.[15, 16] However, corresponding zinc anode reactions are consistent for a specific electrolyte. In recent widely used mildly acidic electrolyte such as $ZnSO_4$, zinc anode reaction is considered as the chemical convention between elemental zinc and zinc ion, that is deposition/stripping of zinc metal accompanying charging/discharging operations (equation 1 and Fig. 1a).[37, 41]

$$Zn\ (s) \rightleftharpoons Zn^{2+}(aq) + 2e^{-} \qquad (1)$$

The thermodynamic driving force for the process can be described by equation 2:[51]

$$\Delta G = zF(\emptyset - \emptyset^{\circ}) = zF\ \eta \qquad (2)$$

Where ΔG is the free energy change for the electrode reaction, F is the Faraday constant, $\emptyset^{\circ}$ is the equilibrium potential for the reaction, η is the overpotential. Due to the existence of overpotential, therefore, the electrochemical reaction in fact is a non-equilibrium state.

One important aspect is to study and monitor the morphology of metal electrodeposition at the electrode interface, which is crucial for the advancement of battery technology. Continuous deposition/stripping of zinc metal could lead to the evolution of electrode-electrolyte interface (i.e. interface shape changes) under the electrical and chemical driving forces. Factually, the electrode interface is not a sharp-interface version as described by the Gouy-Chapman model, but a dynamic interface picture. So, certain theoretical and numerical approaches such as linear or nonlinear phase-field models were developed for understanding the mechanisms of the electrodeposition process especially the dendrite growth process.[51-63] These models provide an effective route to analyze the deposition morphology of zinc metal in different electrolytes. Theoretical and experimental results indicate that certain factors will affect deposition morphology such as substrate, current density, applied voltage and ion concentration. Zinc deposition can form various fractal or dendritic patterns at different electrolyte concentration

View Article Online
DOI: 10.1039/D0EE02079F

and applied voltage.[61, 63] In practical ZIB devices, the dendritic deposits of a zinc anode and related side reactions (HER, corrosion and passivation) mainly caused by free water become two main problems (Fig. 1b), greatly limiting cycling lifespan of ZIBs. The following will discuss the reasons for the two issues and general solving strategies till now.

2.1. Zinc dendrite growth behavior and general solving strategies

It is a common phenomenon that the metal (Li, Zn, etc.) electrodeposition tends to form ramified morphologies, especially dendrite-like deposition.[49] The dendrite growth is closely related with inhomogeneous nucleation caused by non-uniform electron and ion distribution at the interface (Fig. 2). While homogeneous nucleation often need rigorous conditions including smooth electrode surface, homogenously distributed interface electric field, fast ion transfer to the interface, more nucleation sites and so on.[37-48] However, in a real specific electrode interface, the electrode surface is not atomic-level smooth, resulting in uneven charge distribution and nucleation barrier. So zinc ions at interface will preferentially deposited on those higher active sites, forming dispersive zinc crystal nucleus in the initial nucleation process. The deposits of as-formed protrusions further exacerbate the unequal distribution of electrical field and ion flux at interface and finally, slowly increasing the dendrites formation.[38-40] Larger-sized nuclear seeds have a larger impact on electric field distribution and ion distribution based on finite-difference simulation (Fig. 2a-f).[64] So, it is vital to avoid the formation of uneven large-sized zinc nucleus, which more easily caused dendrite growth. Moreover, The dendrite growth is more serious at large current density because of the limited diffusion process at high current density and because there exist critical current density effect (Fig. 2g).[64, 65]

Dendrites can degrade battery performance in several ways. The formation of dendrite can decrease the electron transfer at interface as the loose structure of the dendrite may lower the area of contact. And, worse, this zinc dendrites will possibly fall off from the bulk electrode and thus form dead zinc during cycling of ZIB. Most seriously, the dendrites grow to an extent

View Article Online
DOI: 10.1039/D0EE02079F

can pierce separator to contact cathode causing a short circuit and thus directly cause the failure of battery. Currently, two general strategies are developed for efficiently solving zinc dendrite issue: regulating homogeneous nucleation and inducing epitaxial deposition (Fig. 3). Many methods can be used to realize homogeneous nucleation such as homogenizing electric field distribution, controlling interfacial zinc ion distribution and diffusion behavior, regulating nucleation barrier and nucleation sites.[45-47] Apart from these widely used controlling even nucleation techniques, another effective method is inducing epitaxial nucleation and growth.[49] This method is based on using specific substrate which has a small crystal lattice mismatch with a zinc crystal lattice plane. At this substrate, zinc will grow in parallel to electrode plane, forming a thin film growth pattern, avoiding common dendrites growth models.

2.2. Water-induced side reaction issues and general solving strategies

Apart from the zinc dendrite issue, side reactions mainly caused by water in the electrolyte can also degrade ZIB performance. Compared with alkaline electrolyte (KOH) based ZIBs, the current widely used mildly acid electrolytes ($ZnSO_4$, etc.) show a higher thermodynamic tendency of HER because of higher H^+ activity.[37, 41] Although zinc anode has high overpotential for HER, HER can become a non-negligible competitive reaction with zinc plating/stripping under certain conditions such as low potential and high current density. HER could produce some undesirable results: 1) gas generation of HER will cause gas bubbling/expansion of battery and finally result in leakage of electrolyte; 2) the consumption of H^+ can cause local pH change, forming local alkaline environment, and zinc ion will form insulative chemicals such as $Zn_4(OH)_6SO_4$/ZnO attached on zinc anode (Equation 3-5), worsening the electric contact.

$$2H_2O(l) + 2e^- \rightarrow H_2(g) + 2OH^-(aq) \quad (3)$$

$$4\,Zn^{2+}(aq) + 6OH^-(aq) + SO_4^{2-}(aq) \rightarrow Zn_4SO_4(OH)_6(s) \quad (4)$$

$$Zn^{2+}(aq) + 2OH^-(aq) \rightarrow Zn(OH)_2(s) \rightarrow ZnO(s) + H_2O(l) \quad (5)$$

View Article Online
DOI: 10.1039/D0EE02079F

Therefore, it is also critical for high-performance ZIBs to solve these side-reaction issues. Considering the root of the side reactions is caused by a large number of free water molecules. So, inhibiting free water molecules from reaching an electrode interface or reduce the interfacial water content become the main idea to suppress side reactions.

There are two general strategies including surface coating layer and design novel electrolyte systems with little water content, which can achieve the above objectives. Besides, modifying zinc anode induce higher overpotential for HER is also an effective way to suppress HER.[37] It should be mentioned that dissolved oxygen in electrolyte also impact zinc anode performance,[50] so the coating layer not only inhibits water but also function as a barrier for oxygen diffusion. The dissolved oxygen can also be removed by degassing treatment. It should be noted that zinc dendrite and water-induced side reactions have a clear inner relation. The side reactions may alter the distribution of the electrical field and diffusion of ions at interface, which makes it more likely to form zinc dendrite. In turn, the zinc dendrite will increase the side reactions because zinc dendrites possess local higher-concentration charge distribution and more active sites compared with bulk zinc electrode. This is because zinc dendrite has more low coordination zinc atoms and a more defective crystal lattice plane which can catalyze HER. So, it is necessary to consider the internal relations between zinc dendrite and side reactions for effectively optimizing zinc anode.

3. Material and structure designs towards high-performance zinc anodes

On account of the above analysis, the regulation of nucleation and the suppression of side reactions are two important aspects for the production of stable and dendrite-free zinc deposits and therefore good battery efficiency. For realizing these purposes, it needs to comprehensively control interfacial electron transfer kinetics, ion diffusion modes, as well as water/oxygen content at the interface. These parameters can be controlled by optimizing each part of the battery such as zinc electrode itself, electrolyte and separator. This is because these assembly

components have a close connection with battery performance. In this section, we will detailly discuss the current strategies based on material choosing and structure construction toward high-performance zinc anodes. For clarity, we will analyze and discuss these strategies from four aspects: 1) surface coating layer modification of planar zinc electrode; 2) internal structural optimization of zinc bulk electrode; 3) electrolyte modification and 4) multifunctional separator designs (Fig. 4).

3.1. Surface coating modification of planar Zn anode

Planar zinc anode such as zinc foil/plate owe some merits from an industrial viewpoint because of their easy availability and thus become the most widely used zinc anode. However, pure zinc foil/plate has certain shortcomings. For example, the limited specific area of the planar zinc anode is not beneficial for homogenous electric filed distribution and thus harmful for homogenous nucleation. On the other hand, the simple planar structure easily becomes electrical insulation once the passivation layer is formed on its surface. These shortcomings can be addressed by designing the surface coating layer, which is demonstrated an effective route to enhance zinc anode performance and simultaneously maintain good practicability. The artificial interface layer is similar to solid electrolyte interphase for lithium anode which has a positive effect for anode, not only regulating anode surface electrochemical environment, but also providing physical protective interphase. So, surface modification can act as a multifunctional layer and thus protect or regulate interfacial chemical/electrochemical properties and processes. By this surface engineering based on material and structure designs, zinc anode performance can be effectively enhanced.

Currently, series of advanced materials have been developed as coating materials including metal/metal oxides (sulfides) nano materials (Au, In, ZrO_2, TiO_2, Al_2O_3, ZnO, ZnS), [66-73] inorganic acid salts ($CaCO_3$, kaolin),[74, 75] MOF based materials (ZIF-8, ZIF-7), [76, 77] carbon based materials (graphene oxide, reduced graphene oxide, carbon black, hydrogen-substituted

View Article Online
DOI: 10.1039/D0EE02079F

graphdiyne),[78-81] polymer materials (polyamide, Polyvinyl butyral), [82, 83] and organic-inorganic hybrid materials (polyvinylidene fluoride/TiO_2,Nafion/Zn-X zeolite),[84, 85] Typically, the coating layers can have several roles depending on different materials as well as specific structures (Table 1):[66-85] 1) acting as hetero seeds. Conductive nanoparticles can be homogeneously coated on zinc foil and act as hetero seeds inducing homogeneous deposition of zinc metal; 2) homogenizing charge (electron or ion) distribution of zinc anode surface. Many materials can be used to realize the aim. For example, certain metal oxide with a high dielectric constant can induce surface space charge polarization effect (i.e. Maxwell–Wagner polarization) to form homogenous charge distribution; 3) regulating interfacial zinc ion diffusion behavior. 2D random diffusion of zinc ions at the interface is one critical factor of uniform electrodeposition.[71] The 2D random diffusion will cause preferred deposition phenomenon, exacerbate the uneven distribution of ion flux and finally cause serious dendrite growth; Certain materials can be used as a coating layer to optimize interfacial zinc ion diffusion by different principles such as electrostatic interactions, channel guiding effect; 4) inhibiting interfacial water/oxygen to suppress side reactions. Certain coating layers have a dense structure or strong molecular interactions which can act as a physical barrier to prevent water/oxygen diffusion to electrode interface, and thus decreasing water/oxide content at the interface. Factually, these coating materials often have more than one function as mentioned above and can obviously enhance zinc anode performances (Table 2).

Metal nanoparticles such as Au can be used as hetero seeds to induce uniform deposition of zinc metal. Cui *et al.* reported a quasi-dispersed gold nanoparticle with diameters of about 100 nm coated zinc anode by ion beam sputtering.[66] The Au nanoparticles coating layer almost does not change the wettability between the electrode surface and electrolyte. The high curvature and large local electric field guided homogeneous nucleation and growth of zinc metal, forming disc-like Zn-flake-arrays structure rather than uneven dendrites/protrusions. Electrochemical tests show the decreased voltage polarization after activation in the first cycle, and no obvious

View Article Online
DOI: 10.1039/D0EE02079F

protrusions were found, indicating the uniform deposition of zinc on the Au coated zinc surface. A Zn-MnO_2 full cell of the Au coated zinc anode matched with magnesium oxide show significantly improved cycle life up to 2,000 cycles while bare Zn-based full cell failed after only 480 cycles. After 2000 cycles, the morphologies of the two kinds of zinc anode is sharply different. The Au coated Zn anode still maintain an integral disc structure with array-like deposits, while bare Zn anode has pulverized structure with obvious protrusions deposits.

Other metal such as indium (In) is also demonstrated an effective coating material to improv zinc anode. [67] The In layer can be in situ built by a spontaneous galvanic replacement reaction between Zn metal and $InCl_3$. Because of its good chemical inactivity of –0.338 V vs. the standard hydrogen electrode and high hydrogen evolution overpotential, the In layer can act as a corrosion inhibitor. On the other hand, similar with the Au nanoparticle coating layer, the In layer can also act as nucleating agent because In has a higher adsorption energy for Zn atoms implying Zn atoms will preferentially deposit on it. The two functions of the In layer can not only decrease production of by-products such as $Zn_4SO_4(OH)_6 \cdot 3H_2O$, but also induces the uniform deposition of zinc. The symmetric cell based on the In coated zinc can stably cycle for 500 h under a current density of 1 mA cm^{-2} and 1 mAh cm^{-2}, and 1500 h under a current density of 0.2 mA cm^{-2} and 0.2 mAh cm^{-2}.

Besides metal particle coating layer, series of metal oxides such as ZrO_2, [68] TiO_2, [69] Al_2O_3[70] and ZnO[71, 72] with different dimensions or structures have been used as coating layers to improve deposition/stripping performance of zinc anode. Different from the conductive metal nanoparticle layer, these insulating metal oxides mainly realize optimizing function by regulating interfacial ion behavior. Liang *et al*. reported a ZrO_2 with a diameter of 35 nm as the coating layer prepared by casting ZrO_2/PVDF/NMP slurry (Fig. 5 a-e). The ZrO_2 can provide more nucleation sites by Maxwell–Wagner polarization effect and thus inducing uniform zinc plating. The insulating ZrO_2 layer also produces high overpotential of HER that can suppress HER side reaction, inhibit corrosion and zinc-anode passivation. Asymmetric cell tests

View Article Online
DOI: 10.1039/D0EE02079F

demonstrate the ZrO_2 coated Zn anode show low nucleation overpotential and uniform nucleation behavior. Even at a high current density of 20 mA cm^{-2} and corresponding areal capacity of 5 mAh cm^{-2}, the ZrO_2 coated Zn anode still has high Columbic efficiency of 99.85% and cycling stability above 200 cycles. Symmetric cell shows low polarization of only 38 mV, and long cycling life up to 3800 h at 0.25 mA cm^{-2} and corresponding areal capacity of 0.125 mAh cm^{-2} (Fig. 5e). At a high current density of 5 mA cm^{-2} and areal capacity of 1 mAh cm^{-2}, the ZrO_2 coated Zn anode can cycle for more than 2100 h, while pure Zn anode can only cycle for 100 h. Morphology analysis after 100 cycles at 5 mA cm^{-2} and 2.5 mAh cm^{-2} demonstrate the smooth deposition surface of ZrO_2 coated Zn anode (Fig. 5 c, d), while bare zinc anode occurs surface cracking and pulverization (Fig. 5 a, b). The enhanced performance should be attributed to the enhanced nucleation sites by space charge polarization, reduced the contact area between zinc and electrolyte which avoids a series of side reactions including corrosion, passivation and HER.

Metal oxide (TiO_2, Al_2O_3) [69, 70] coating layer especially the molecule level thin coating layer can also be constructed by specific techniques such as atomic layer deposition. For example, a highly stable zinc metal anode was fabricated by Al_2O_3 coating. The ultrathin Al_2O_3 layer was obtained via an atomic layer deposition technique and suitable thickness is controlled. The effect of Al_2O_3 coating thickness on zinc anode performance shows the $100Al_2O_3$@Zn is better than other counterparts including $30Al_2O_3$@Zn, $60Al_2O_3$@Zn and $200Al_2O_3$@Zn. The ultrathin Al_2O_3 layer (10 nm) reduces the contact angle of bare zinc anode surface from 88 to 71° (3M $Zn(SO_3CF_3)_2$ aqueous solution as electrolyte), indicating the surface wettability of Al_2O_3 coated zinc anode is enhanced which will be helpful for more even Zn ion flux as well as favorable charge transfer kinetics during deposition/stripping of zinc metal. Besides these, the Al_2O_3 layer alleviates the corrosion of zinc anode in aqueous electrolyte media. The corrosion potential of Al_2O_3 layer coated Zn foil become more negative and the corrosion current fell by almost half. This effect is further confirmed by a reduced content of $Zn(OH)_2$

View Article Online
DOI: 10.1039/D0EE02079F

byproduct formed in the cycling process of Zn|Zn symmetric cells. These multiple roles ultimately improved Zn stripping/plating reversibility, prolonged cycling lifespan up to 500 h at current density of 1 mA cm^{-2} and areal capacity of 1 mAh cm^{-2}, and thus generate high-performance full cell in which δ-MnO_2 as the cathode.

Besides these metal oxide particle coating, 3D porous metal oxide architecture is also an effective coating layer which improves the surface electrochemical reaction of the zinc anode. Xie *et al*. constructed a 3D nanoporous ZnO network on the surface of the zinc plate through in situ solution phase deposition of $Zn(OH)_4^{2-}$.[71] This 3D metal oxide coating layer can reduce the local current density and avoid the "tip effect" by homogenizing the 3D distribution of electric field. In addition, this ZnO architecture enhances the electrostatic attraction to zinc ions and makes the zinc ions in the interfacial double layer have low desolvation energy, thus accelerating the transfer and deposition kinetics of zinc ions and reducing the deposition overpotential. This 3D ZnO enhanced interfacial structure not only effectively inhibits the formation of zinc dendrite, but also suppress side reaction of HER, realizing the high utilization ratio up to 99.55% and long cycle life of zinc anode.

MOF-based materials can also be used as a coating layer to enhanced zinc anode performance via specific chemical composition and porous structure. For example, ZIF-8 can be in situ growth on zinc surface and/or then fast thermal treatment to form N doped porous carbon networks.[76] These structures obtained by the in situ route have a close contact, which avoid dendrite growth at the interfacial gap and can improve the capacity of ZIBs. The ZIF-8 and carbonized ZIF-8 structure showed improved wettability, indicating increased hydrophilicity, which was conducive to the formation of uniform deposition of zinc ions on the anode surface. Symmetrical cells with a 2 M $ZnSO_4$ electrolyte showed that with the increase of current density, the performance of pure Zn anode was gradually weakened, while the MOF-based materials modified zinc anode still show low voltage hysteresis and high stability. Consequently, no zinc dendrite was observed in the MOF modified zinc anode, indicating that the MOF-based

View Article Online
DOI: 10.1039/D0EE02079F

materials promote the homogeneous deposition of zinc. This uniform plating is attributed to coordination effect between ZIF-8 and zinc ions which is conducive to the diffusion of zinc ions, uniform distribution of interfacial charge. Also, functional groups with rich N and O elements formed by pyrolysis are conducive to the migration of zinc ions in the porous coating layer.

Diverse carbon-based materials, including reduced graphene oxide (rGO),[79] carbon black[80] and hydrogen-substituted graphdiyne (HsGDY)[81] are also studies with the excellent properties as a coating layer to improve the zinc anode performance. Graphene materials have high mechanical strength that can be used to suppress the growth of zinc dendrite. The use of reductivity of zinc metal towards the graphene oxide precursor can easily produce a rGO-coated zinc anode.[79] Electrochemical performances of the symmetric cell assembled by the rGO coated zinc anode show greatly reduced overpotential and voltage hysteresis and can stable cycling for 200 cycles at different current densities ranging from 1 to 10 mA cm^{-2} at the areal capacity of 2 mAh cm^{-2}. The improved zinc anode is due to the excellent conductivity of the rGO layer that reduces interface resistance and inhibits the formation of zinc dendrite. In addition, 2D graphdiyne material has excellent physical/chemical characteristics and is used widely for electrochemical energy storage. A HsGDY coated zinc anode was constructed by Yang *et al*. to optimize the zinc anode performance with a commercial-level loading mass.[81] Together, HsGDY can in situ grow onto a zinc surface thanks to a simple liquid phase synthesis technique of HsGDY, which forms rather uniform and stable coating layer, thus avoiding potential pulverization scarcity of common slurry coated coatings. Besides its strong chemical stability, the HsGDY offers ion tunnels at a level sub-ångström derived from their unique structure that allow zinc ion concentration redistribution to be regulated, thus eliminating zinc dendrite. Symmetric cells assembled by the Zn@HsGDY electrode demonstrate the greatly enhanced lifespans up to 2400 h at different current densities of 0.5, 1 and 2 mA cm^{-2}, which is dozens of times high than pure zinc counterparts. The full battery assembled by an N-doped porous

carbon cathode and Zn@HsGDY anode can stably cycle for a long time up to 10 000 cycles at high cathode loading mass of 22.95 mg cm^{-2} which is comparable with commercial-grade criteria. This work provides a valuable reference for designing dendrite suppression strategies which take into account the zinc anode performances under commercial-grade loading mass.

Commercial carbon materials like carbon black (CB) can also improve the performance of zinc anode by acting as a coating layer. Wang *et al*. developed a zinc anode based on coating the conventional zinc foil anode with carbon black and nanofibrillated cellulose (NFC) binder.[80] The CB component provides an electrically conducting network to expand the electroactive surface and to create a large amount of voids for accommodating the zinc plating sources with the spherical shape structure. The NFC component can facilitate charge transport because of its electrolyte reservoir function. Symmetric cell tests show that the CB-NFC coated zinc foil anode possess lower polarization than the pure zinc foil counterpart (160 mV vs. 280 mV), and prolonged cycle lifespan up to 400 h (vs. 60 h for pure zinc anode) without voltage fluctuation at the current density of 0.5 mA cm^{-2}. The effectiveness and practicality of the CB-NFC modified zinc foil anode is demonstrated by the equivalent cycle performances up to 400 h at a commercial-level areal capacity of 5 mAh cm^{-2} at the current density of 5 mA cm^{-2}.

Organic polymers have rich functional groups that can interact with metal ions, and also have an excellent property of film-forming. Polymers provide potentially covering materials for zinc anode modification to direct uniform zinc metal deposition and prevent side reactions. Inspired by brighteners principles in sophisticated surface electroplating technology of zinc, Zhao *et al.* used polyamide (PA) as effective coating layer to improve zinc anode performance in terms of long-life and deeply rechargeability (Fig. 5 f-h).[82] The PA coating layer was obtained by casting the solution of PA and $Zn(TfO)_2$ in anhydrous formic acid onto zinc foil and then dried to remove formic acid. The PA interphase has a strong interface binding effect, chemical stability and excellent mechanical toughness/flexibility. Moreover, the rich polar amide groups in PA molecules provide hydrogen bonding ability and coordination sites. Thus, the PA coating layer

View Article Online
DOI: 10.1039/D0EE02079F

not only prevents the penetration of water/oxygen but also reduces the free water content of the zinc surface through hydrogen bonding functions. The numerous amide coordination sites in PA molecules can, on the other hand, efficiently boost interaction with zinc ions and thus alter the zinc ion distribution and transportation at the interface layer. This optimized uniform distribution of zinc ion at the interface is vital for the homogenous deposition of zinc metal. Although the strong interaction between PA and zinc ion can increase polarization and nucleation overpotential, it can also in return increase nucleation active sites and homogenize grain size, and eventually, avoid zinc dendrite issues.

Electrochemical tests demonstrated the reduced side reactions (HER, corrosion) and restricted two-dimensional random diffusion of zinc ion at the electrode interface. In situ optical microscopy shows the dendrite-free plating/stripping pattern of zinc in the PA coated zinc electrode interface (Fig. 5 g), while obvious dendrite growth occurs for pure zinc anode. The symmetric cell of the PA coated zinc anode shows long-term galvanostatic cycling up to 8000 h at a current density of 0.5 mA cm^{-2} with changeless voltage curves, indicating excellent reversibility of plating/stripping (Fig. 5 h). The enhanced performance reaches 60-fold improvement compared with a bare zinc anode. Moreover, high reversibility and long cycle life of the PA coated zinc anode can still be retained at 85% theoretical depth of discharge state. Full prototype cells assembled using the PA modified zinc anode with α-MnO_2 show obviously enhance cycling life up to 1000 cycles and the morphology after cycling shows dendrite-free zinc deposits, further confirming the effectiveness of PA coating. Considering the easy availability of PA material and simple solution casting technique, the method not only enhanced zinc anode performance but also provided a cost-efficient, facile and scalable approach, which well follows the original low-cost nature of aqueous ZIBs.

Certain porous coating materials possess narrow channels which can generate specific ion regulating/sieving effect. For example, sub-nanometer-sized pore in certain MOF materials can be used as a coating layer with a sieving role to control solvation structures of zinc ions (Fig.

View Article Online
DOI: 10.1039/D0EE02079F

6a, b). [77] ZIF-7 was reported as a coating layer to make hydrated zinc ions desolvation in advance before reaching the interface, forming a super-saturated electrolyte front surface layer, realizing improved plating/stripping stability of zinc anode (Fig. 6c).[71] The ZIF-7 was cast onto Zn foil by the doctor blading technique and used as the front surface layer. Because of the narrow channels in ZIF-7 with size windows ca. 2.94 Å, normal solvated zinc ion in the bulk electrolyte will partly desolvate after entering into the channels driven by the electric field. Different from the typical hydrated zinc ion, the solvated zinc ion in ZIF-7 channels become unique ion complexes such as H_2O-Zn^{2+}-OSO_3^{2-}. The ionic association structure means the free water content in the MOF channel as well as electrode surface decreased significantly, thus avoiding the water-induced side reactions and dendritic deposition of zinc anode. Symmetric cells based on ZIF-7 coated zinc anode can survive up to 3000 hours (125 days) at 0.5 mA cm^{-2}, while bare zinc anode-based cell can only cycle for 55 h (Fig. 6d). Besides, the morphology of zinc deposits become round-edged and dense-packed mode after ZIF-7 coating, which is different from typical zinc dendrite mode in bare zinc case. And the ZIF-7 coated zinc anode only has fewer side products of ZnO, $Zn(OH)_2$ which can only be detected in the surface of deposits. While bare zinc anode shows obvious signals of those side products in both surface and interior of deposits. These results confirm the MOF coating layer can efficiently reduce the free water content reaching the zinc anode surface and guide the dendrite-free deposition of zinc. Full cells of Zn-MnO_2 based on the ZIF-7 coated zinc foil show high stability with high capacity retention of up to 88.9% after 600 cycles.

Other porous materials such as kaolin ($Al_2Si_2O_5(OH)_4$) can also improve zinc deposition by specific pore dominated regulating effect.[75] Kaolin has a uniform porous structure with a narrow pore size distribution of 3 nm and a sieving function towards zinc ion (Fig. 6e). So, it can induce uniform migration and deposition of zinc ions which is beneficial for suppressing zinc dendrite. Chronoamperometry shows the kaolin coating can change the original disordered two-dimensional diffusion behavior of zinc ions at interface into a stable three-dimensional diffusion

model. Besides, the kaolin can also reduce the self-corrosion of zinc anode which can be confirmed by reduced corrosion current density of zinc anode based on Tafel polarization curve. Consequently, zinc deposits show smooth morphologies and the dendrite-free morphology can still maintain after 10, 20 and 600 cycles for kaolin coated zinc anode. This optimized electrochemical deposition behaviour ensures long-term cycling capacity up to 800 h at 4.4 mA cm^{-2} and 1.1 mAh cm^{-2} (Fig. 6f). This enhanced performance is attributed to the porous structure of kaolin which has selective chemical adsorption toward zinc ions.

In general, often used inorganic coating layers clearly can diminish the zinc stripping/plating polarization potential due to the unimpeded channels provide for ion transportation.[66-75] These inorganic layers of layering, however, composed in particular of particulate matter, such as nanoparticles with metal oxide, have low mechanical strength and adhesion, so that they can deform after a long cycle of zinc plating/stripping. In contrast, organic film-forming properties like PA have excellent mechanical and adhesive properties. However, because of increased nucleation barrier and limited ion diffusion, the substantial hydrophobicity of some polymers could lead to increased polarization for Zn plating/stripping.[82, 84] Researchers suggested effective methods for resolving these problems. For example, in situ coating techniques can effectively solve the unsatisfactory surface adhesion of inorganic coating materials. For constructing a strong adhesive and high transference numbers of Zn ion coating layer, Hao *et al*. developed a in situ vapor–solid strategy to build an artificial interphase of ZnS.[73] Calculations of the density functional theory (DFT) show that, by stemming from charge migration, S atoms in ZnS have a strong binding interaction with zinc atoms. The interaction of charges not only facilitates Zn^{2+} diffusion at the interphase but also increases the ZnS layer's adhesion to the Zn substrate. The ZnS interphase permits dendrite-free Zn deposition thanks to its excellent mechanical strength and high ion conductivity. The symmetrical cells based on the ZnS modified zinc anode show prolonged cycling stability for above 1100 h at 2 mA cm^{-2} and 2 mAh cm^{-2}, much larger than bare zinc case of only 100 h.

Apart from adopting a strategy for in-situ coating, an organic-inorganic hybrid strategy that uses the beneficial properties of polymer and inorganic materials has also been developed. Recently Cui *et al.* developed an organic-inorganic hybrid coating layer in which Zn-X zeolite was combined with Nafion.[85] The co-ordination of zinc ions in Zn-X and Nafion (-SO3-) in this hybrid coating layer provides a well-bridged organic-inorganic interface. Zn-X zeolite has smaller pore size of below 0.74 nm which is much smaller than those channel size in Nafion of 4nm, implying anions can be effectively hindered while zinc ion can travel freely on the surface/inter surface of Zn-X zeolite. Ion permeability test demonstrates the screen effect of Zn-X component toward SO_4^{2-} anions, whose permeability value decrease from 2.04×10^{-9} cm^2 s^{-1} for Nafion layer to 0.61×10^{-9} cm^2 s^{-1} after adding 5wt% Zn-X. On the other hand, the coordination of zinc ion with $R\text{-}SO_3$ in Nafion can effectively reduce the Zn^{2+} desolvation energy which helps improve the kinetics and uniform growth of Zn plating. Symmetric battery tests show the Zn@Nafion-Zn-X anode exhibits much better cycling stability (1000 h at 1 mA cm^{-2} and deep Zn plating/stripping capacity of 10 mAh cm^{-2}) than Zn@Nafion anode and Zn@Zn-X anode, and simultaneously much lower polarization (50 mV) than bare zinc of 90 mV, indicating the good depolarization effects of Nafion based coating layers. This paper provides a good reference to the building of a rational coating layer, which can freely transport zinc ions but block water molecules and other ions.

It can be seen that different materials including conductive, insulative, inorganic, organic materials and unique porous materials can be used as coating layers to improve zinc anode performance mainly in terms of enhanced Columbic efficiency, polarization and especially cycling lifespan. It should be mentioned that for constructing an effective coating layer, certain factors should be noticed such as the thickness of the coating layer, which has been demonstrated as an essential factor for the final effect. Although a thicker coating layer can enhance inhibit for water and dissolved oxygen, excessive coating layer can increase the difficulty for ion diffusion and degrade electrochemical performances of zinc anodes either.

View Article Online
DOI: 10.1039/D0EE02079F

Besides, sufficient mechanical strength and good interface bonding of coating layer is also needed.

3.2. Internal structure optimization of zinc electrodes

Apart from surface engineering toward planar zinc anode architecture, modifying the internal structure of the zinc bulk electrode is another effective route to construct high-performance zinc anode systems. Optimizing the composition of zinc electrode and creating different structures can enhance the electrochemical performances of ZIB. The internal zinc bulk structure optimization can classify several forms such as 3D network hosted zinc anode, zinc alloy anodes and specific substrate-induced epitaxial zinc anode.[86-103, 49] 3D network hosted zinc anodes can generate enhanced performances compared with common planar zinc anode such as zinc foil or zinc plate. For example, 3D zinc sponge can obviously enhance battery performance mainly because of its stronger charge transfer network.[86, 87] Apart from the pure 3D zinc anode, the most common strategy is to construct composite 3D zinc structures. For example, some 3D materials skeletons can be used as hosts to support zinc, forming 3D hybrid zinc anodes.[88-100] The 3D hosts can be various materials such as carbon materials (graphene foam, CNT networks, carbon fibers), [88-94] metal materials (porous copper, copper foam, steel mesh),[97-100] metal-organic frameworks (MOF) derived materials (ZIF-8 derivatives) [95] and MXenes.[96] In addition, constructing zinc alloy is another effective strategy to optimize zinc anode performance.[101-103] Zinc can form alloys with a variety of metals such as aluminum, copper. Alloying can effectively regulate zinc crystal structure and surface properties, which can provide a better interface for nucleation and simultaneously suppress side reactions. Besides these, a specific substrate such as graphene induced epitaxial zinc anode is also an effective strategy to improve zinc anode performance.[49] Such material and structural design techniques help to homogenize the distributed electric fields, decrease nucleation over-potential, increase

zincophilicity and nucleation sites, and regulate the zinc growth orientation, and are therefore beneficial for the development of high-performance zinc anodes (Table 3).

3.2.1 3D framework hosted zinc anode

A series of materials such as carbon materials, MOF based materials and metal materials can be used as hosts for constructing 3D composite zinc anodes because these materials can form 3D porous network structures. The 3D composite zinc anodes have a large surface area which can form uniform electric field distribution and dispersing current density which might avoid critical current density of dendrite growth. Apart from the homogenous electric filed distribution, the large contact area with electrolyte is also helpful for the homogeneous ion concentration distribution. Besides these, the 3D porous skeleton can confine zinc dendrite growth in a 3D space and thus reduce the risk of short-circuit by piercing separator to a certain degree.

Carbon materials with 3D porous structures are widely used as hosts in battery fields for preparing 3D structured electrodes. This is attributed to carbon materials have large specific surface areas, excellent conductivity and electrochemical inertness. Carbon network host zinc anode can effectively homogenize electric field distribution, decrease zinc nucleation overpotential and size, and thus the multifunctionality of carbon hosts can alleviate zinc dendrite growth. Several carbon materials including 3D carbon nanotube networks[90, 91], graphene foam[93], carbon fiber[88, 89], Tin-modified 3D carbon felt[92] have been tested as hosts for zinc anode for improving homogeneous deposition behavior of zinc metal.

For example, Zeng *et al.* used highly conductive CNT frameworks for dendrite-free zinc deposition (Fig. 7).[90] The disordered CNT array was constructed on a carbon cloth by chemical vapor deposition, and the impurity-free Zn/CNT anode was obtained by electrodeposition (Fig. 7a-c). Electrochemical results show that the Zn/CNT anode has significantly improved electrochemical performance in terms of lower voltage polarization (30 mV vs. 70 mV) and

View Article Online
DOI: 10.1039/D0EE02079F

longer cycling life (400 h vs. 20 h) compared with those zinc anode deposited on pure carbon cloth (Zn/CC), indicating that the CNT framework plays a key role in zinc deposition performance (Fig. 7e). The nucleation overpotential of Zn/CNT anode is 84 mV, much lower than that of Zn/CC (192 mV). The deposition morphology of Zn/CNT anode show much uniform deposition morphology. For further understanding the mechanism of CNT toward zinc plating/stripping behavior. A Maxwell software was used to simulate the electric field distribution of after zinc nucleation on pure CC and CNT networks. The results showed that there was a higher electric charge distribution near the zinc nucleation site on CC, resulting in an uneven electric field and subsequent dendritic deposition. On the contrary, CNT induces a smaller size of zinc nucleation due to its large surface area, leading to a more uniform electric field distribution, avoiding the tip effect (Fig. 7d). The full battery based on the Zn/CNT anode matched with a CNT-MnOx@poly(3,4-ethylenedioxythiophene) (PEDOT) cathode shows enhanced rate and cycling performance and the quasi-solid-state Zn/MnO_2 battery also shows excellent flexibility.

Although pure carbon hosts can provide 3D porous skeleton, one drawback of the carbon materials is low-affinity interaction toward zinc because of pure carbon composition, which is not beneficial for deposition kinetics of zinc ion. A certain method for modifying carbon materials to enhance their zincophilicity is therefore created. Yin *et al*. reported a tin (Sn)-modified 3D carbon felt host (SH) for zinc anode (Fig. 7f-i).[92] Sn was modified on carbon felt by magnetron sputtering and the Sn modified carbon felt does not change the porosity and structure of the carbon felt, so it does not affect the mass transfer process. Sn modification can have multiple functions. On one hand, the Sn provides more nucleation sites and lower nucleation overpotential for zinc deposition and thus can induce uniform deposition of zinc. On the other hand, the Sn component can provide higher hydrogen evolution overpotential which is helpful for further enhancement of battery performance. Deposition morphology analysis shows that zinc deposits on pristine carbon felt host (PH) are scattered, loose, and uneven (Fig.

7f). On the contrary, the plating morphology after Sn modification becomes remarkably homogeneous (Fig. 7g). The superfine surface morphology measurement further confirms that the morphology of zinc deposition on Sn-modified carbon felt remained uniform over time, while the morphology of zinc deposition on pure carbon felt was not uniform, and the height of Zn particles increased unevenly with time. DFT calculations indicate that Sn has stronger adsorption for Zn than carbon (Fig. 7h), resulting in decreased deposition overpotential of zinc (decreased by 20 mV), increased HER overpotential (from -1.54 V to -1.62 V) and enhanced cycling lifespan under large current densities and areal capacities (Fig. 7i). The enhanced performance mainly benefited from the strong interaction of Sn and Zn ion which can induce homogenous nucleation, and suppress side reactions.

MOF is also a porous material used in battery fields, similar to 3D carbons. In addition to the large areas, MOF can provide specific chemical composition, and by thermal treatment, MOF can easily turn into a 3D conductive skeleton. So, it is a favorable host for zinc anode. Xia's group reported a highly stable and reversible zinc anode, which benefits from porous structure, trace zinc remains in the MOF skeleton after thermal treatment, and the high HER overpotential (Fig. 8).[95] The temperature of heat treatment is an essential factor for obtaining an ideal MOF-based host. It has been found that thermal treated ZIF-8 at 500 ^{o}C (ZIF-500) is the best candidate for hosting zinc because the temperature not only can maintain the intrinsic porous structure of original ZIF-8 but also can moderately thermal reduce zinc ions of ZIF-8 into uniformly distributed elemental zinc which can act as nucleation sites, inducing homogeneous deposition of zinc (Fig. 8a). Excessive temperatures between 500-800 ^{o}C can result in a serious decrease in the amount of elemental zinc because of zinc volatilization at higher temperatures. The ZIF-500 hosted zinc anode has the highest Coulombic efficiency (98.6-99.8%%) and cyclic stability at a wide range of current densities and deposition capacities, indicating the best reversibility of zinc deposition in the ZIF-500 system (Fig. 8b, c). The morphology of zinc deposition remains smooth under different deposition areal capacities (Fig. 8d, e). The ZIF-500 hosted Zn

View Article Online
DOI: 10.1039/D0EE02079F

anode matched with activated carbon or I_2 cathodes, forming electrochemical hybrid capacitor and battery, all show enhanced electrochemical performances.

3D metal materials such as porous copper skeleton can support zinc metal for enhanced plating/stripping performances of zinc anode.[100] The 3D copper hosted zinc anode is fabricated by electrodepositing zinc on chemically etched porous copper networks. The 3D porous zinc anode enables the uniform deposition/stripping of zinc, resulting in reduced polarization, stable cycling performance, and almost 100% Coulombic efficiency. Symmetric cells based on the 3D zinc electrode show small voltage hysteresis of only ~40 mV, and long cycling stability up to 350 h at the current density of 0.5 mA/cm^2 and areal capacity of 0.5 mAh/cm^2, which is better than that of planar zinc foil counterpart with larger voltage hysteresis (100 mV) and short cycling lifespan (110 h). After long-term cycles, the morphology of the 3D Zn electrodes can remain intact while the planar zinc foil electrode shows unstable deposition process and defective appearance with large zinc protrusions/dendrites and by-products. This enhanced mechanism is attributed to the multifunctional 3D copper skeleton which can always maintain high electrical conductivity and simultaneously effectively accommodate the volume change of Zn anode during plating/stripping processes.

Besides, various common metal foam/mesh are also usable matrixes for hosting zinc anode.[97-99] Moreover, the metal materials have excellent practical value because of their wide commercial application in the battery field. Metal hosts may be of assistance directly to the use of zinc anodes in operation. Metal types and their structure could affect the plating/stripping performance of zinc. Zhou's group studied zinc deposition performance on various metal hosts/substrates with specific structures such as Cu foam, Cu foil, Ni foam, steel foil and steel mesh (Fig. 9a-c).[97, 98] Compared with other metal such as nickel and steel, copper substrate has a smaller nucleation barrier for zinc deposition because of strong zincophilicity of copper while steel owns the highest nucleation energy barrier (Fig. 9j). Besides, copper shows low self-discharge because of its high redox potential (0.342 V). Although nickel has stronger

View Article Online
DOI: 10.1039/D0EE02079F

zincophilicity for zinc than copper, it can catalyze for HER and result in severe self-discharge, which giving high polarization in symmetry cells and undesirable zinc deposition performance. Among copper substrates including copper foil and copper foam, it has been found that copper foam provides better performance in terms of lower nucleation overpotential, prolonged cycling lifespan (Fig. 9k, l), more uniform deposition morphology, higher Coulombic efficiency, and weaker self-discharge. This excellent anode performance is attributed to the multifunctionality of the 3D copper host in terms of high electrical conductivity, spatially uniform 3D structure, efficient ion transport and high stability in a weakly acidic electrolyte. Full cells assembled by copper foam hosted zinc anode and magnesium oxide cathode show small charge transfer resistance, high rate and cycling stability up to 600 cycles. So, the copper foam should be a better choice for constructing improved zinc anode for constructing high-performance ZIBs.

3.2.2 Zinc alloy anode

Another strategy to optimize zinc bulk structure is constructing zinc alloys. Although various structures of zinc alloy have been designed to improve the efficiency of zinc anodes, most of them targeted at alkaline zinc-based batteries.[33] For currently studied ZIBs, the used mildly acidic electrolytes provide different chemical environments, so zinc alloying strategy should be adapted to the new electrolyte system. Recently, zinc alloy such as zinc–aluminum (Zn-Al) alloy is reported to optimize zinc anode performance. Wang *et al*. constructed a lamella-nanostructured eutectic Zn-Al alloy to realize reversible and dendrite-free anodes for aqueous ZIBs (Fig. 10). [101] In order to effectively boost zinc anode performance, the suitable alloy content for Zn Al alloying and unique Zn-Al alloy design are important. They compared two kinds of Zn-Al alloys: eutectic $Zn_{88}Al_{12}$ alloy and hypoeutectic $Zn_{50}Al_{50}$. The Zn-Al alloys are prepared by the metallurgical process. Different from the disordered structure of hypoeutectic $Zn_{50}Al_{50}$, the eutectic $Zn_{88}Al_{12}$ alloy has an ordered layered structure (Fig. 10a, b). The alternating arrangement of Zn and Al thin layers in the eutectic $Zn_{88}Al_{12}$ alloy is demonstrated

View Article Online
DOI: 10.1039/D0EE02079F

as an effective structure to improve zinc deposition/stripping behavior (Fig. 10c, d). In the $Zn_{88}Al_{12}$ alloy, the zinc component provides the Zn^{2+} carrier, and the aluminum component serves as the 2D skeleton to accommodate the Zn deposition. The insulating layer of alumina on the surface of aluminum prevented electron transfer between Al and Zn^{2+} and induced uniform deposition of zinc between the layers (Fig. 10e, f). The stronger oxidation-resistance of the eutectic $Zn_{88}Al_{12}$ alloy enables better electron transfer and facilitates the zinc deposition/stripping process. The eutectic $Zn_{88}Al_{12}$ alloy anode can still maintain a smooth surface after 2000 cycles at 0.5 mA cm^{-2}, while hypoeutectic $Zn_{50}Al_{50}$ alloy and monometallic zinc all changed to porous and dendritic morphologies. Symmetric cells show that the nucleation overpotential of $Zn_{88}Al_{12}$ alloy is only 20 mV, much smaller than that of monometallic zinc of 108 mV, implying the alloying greatly enhance electronic structure of the electrode. Furthermore, a full cell assembled by the $Zn_{88}Al_{12}$ alloy anode patched with $KxMnO_2$ cathode show rather stable cycling stability with capacity retention of near 100% during 200 cycles at 0.5 A/g. The excellent electrochemical performance of the eutectic $Zn_{88}Al_{12}$ alloy anode indicates that rationally manipulate zinc alloy composition as well as its structure is vital for obtaining desirable effects.

Apart from Zn-Al alloy, copper can also be combined with Zn forming Zn-Cu alloy. Liu *et al*. reported a 3D Zn–Cu Alloy with ordered porous structure prepared by thermal and electrochemical treatment of brass (a common Cu-Zn alloy).[102] The 3D porous architecture enables fast ion and electron transfer, which is beneficial for uniform deposition/stripping behaviour and thus extending the lifespan of the Zn electrode. In contrast with planar Zn–Cu alloy, the 3D structured Zn–Cu anode can give ultrastable depositing/ stripping of zinc metal for above 300 h at 2 mA cm^{-2}, and with small voltage hysteresis and negligible fluctuations in the V-t curves, implying fast charge transfer kinetics and stable electrode structure. The 3D alloy design effectively suppresses dendrite growth, shape change and surface passivation of

Zn anode. Furthermore, High-voltage aqueous Zn–Br_2 battery can be fabricated based on the 3D Zn–Cu Alloy anode and can deliver a high areal specific capacity of about 1.56 mAh cm^{-2}, which can be comparable with commercial Li-ion batteries (≈1–3 mAh cm^{-2}). Copper is favorable material for zinc deposition because it has high zincophilicity and can offer low nucleation overpotential as mentioned above. Moreover, the additional porous structure of the Zn–Cu alloy further improves zinc anode performance.

Zinc soaked in mild acidic medium such as a widely used $ZnSO_4$ electrolyte can result in electrode corrosion during resting and cycling, forming side-products such as insulative $Zn_4(OH)_6SO_4$ layers, hydrogen gas and inhomogeneous corrosion pits. These problems lead to an inevitable increase in electrochemical impedance and greatly prevent the use of aqueous ZIBs in practice. A Cu-Zn alloy/Zn composite was developed to enhance zinc anode performance, to effectively resolve the corrosion issue of zinc metal anode in aqueous electrolytes.[103] The Cu-Zn nanoalloy/Zn anode is obtained with a first replacement of zinc and $CuCl_2$, after an electrochemical conversion while cycling batteries. The chemically inert metallic Cu in the Cu-Zn alloy/Zn anode can improve the anti-corrosive property of the zinc electrode because of its more positive electrode potential (+0.34 V vs. SHE). In addition, Cu has a higher zincophilicity than zinc itself that promotes zinc metal deposition. Linear polarization measurements of the Cu-Zn alloy/Zn anode in 3M $ZnSO_4$ electrolyte show increased corrosion potential (-0.964 V vs. -0.976 V) and greatly reduced corrosion current (6.03 μA/cm^2 vs. 37.15 μA/cm^2), implying the weakened corrosion rate and improved chemical stability of the Cu integrated Zn anodes. Cu/Zn||Cu/Zn symmetric cells further demonstrated the improved electrochemical performances in terms of longer cycling lifespan up to 1500 h at the current density of 1 mA/cm^2 and areal capacity of 0.5 mAh/cm^2.

3.2.3 Graphene substrate guided epitaxial zinc anode

Different from common methods based on inducing homogeneous nucleation to suppress dendrite growth mode, inducing epitaxial zinc anode as a unique strategy is also an effective route to solve zinc dendrite and realize high-performance zinc anode. The Lynden A. Archer group recently published a new notion of epitaxial electrodeposition and found that the graphene substrate could direct zinc metal anode's epitaxial growth patterns. (Fig. 11).[49] This method fundamentally altered the tendency of a metal to form irregular non-planar electrodeposition at the liquid-solid interface. The as-obtained morphology of metal electrodeposition is a film-like structure rather than ramified structures.

The intrinsic reason for graphene substrate can induce the epitaxial electrodeposition of zinc metal is essentially due to the existence of a similar atomic arrangement between graphene and zinc metal, resulting in a low lattice mismatch. The lattice mismatch between graphene (0002) and zinc (0002) is about 7%, well below the empirical value of 25%, implying that metallic zinc can form a semi-coherent interface on graphene crystal plane. Thus, during the electrodeposition process, zinc metal will nucleate and grow along the direction of the graphene crystal plane, forming an epitaxial layer with the same orientation of the graphene substrate. Such oriented nucleation and growth behavior fundamentally avoid the disordered dendrite growth pattern of zinc metal. Apart from the intrinsic reason for low lattice mismatch, another key factor is ensuring the orientation arrangement of graphene sheets in macroscopic graphene substrate. This horizontally arranged (i.e. parallel to the electrode surface) graphene substrate can be obtained by specific processing techniques based on the rheological properties of graphene dispersion. For example, the doctor blade method can be used to induce orientation of disorderly dispersed two-dimensional graphene sheets in a liquid medium such as N-methyl-2-pyrrolidone by applying shear action, thus forming oriented graphene film substrate.

Electrochemical tests showed that the reversibility of epitaxial zinc anode was significantly improved, and the Coulomb efficiency of deposition/stripping reached over 99% after 1000 cycles. This high reversibility of the epitaxial zinc anode facilitates the assembly of

View Article Online
DOI: 10.1039/D0EE02079F

rechargeable batteries with a low negative/positive capacity ratio (N:P). As an example, full cells based on the epitaxial zinc anode matching with MnO_2 cathode with N: P = 2:1 showed good retention capacity after cycling 1000 cycles at the current density of 8 mA cm^{-2}, which is obviously superior to those full cells using zinc anode coated on stainless steel substrate (N: P to 2:1) and 620 microns thick zinc foil (N: P to 350:1) as anodes.

3.3 Electrolyte modification

As a part of the battery, the electrolyte is vital for a cell because its chemical composition directly affects the diffusion behavior and electrochemical reactions of zinc ions. Thus, the optimization of electrolyte components may have a beneficial effect on the interfacial chemistry and the dendrite-free-zinc deposition, resulting in enhanced zinc anode performance (Table 4). Generally, two strategies including electrolyte additives and water-starved electrolyte have been developed to guide the uniform deposition of zinc.[104-114] Typically, electrolyte modification can produce several roles: 1) shielding excessive electric field of initial uneven deposits; 2) regulating the uniform distribution of zinc ion at the interface by electrostatic interaction; 3) guiding the growth orientation of zinc crystals; 4) decreasing free water content to suppress side reactions; 5) changing solvate structure of zinc.

Introducing additives into electrolytes is the simplest way to adjust the composition and affect the electrodeposition of zinc via different roles. Numerous organic small molecules or macromolecules can be used as additives (Fig. 12a, c, e and g). For instance, a certain amount (2 vol%) of ether added into 3 M $Zn(CF_3SO_3)_2$ electrolyte with 0.1 M $Mn(CF_3SO_3)_2$ containing can obviously improve battery performance of Zn-MnO_2.[104] This is because the polarity of ether molecules makes them preferentially adsorbed on initially formed small-sized zinc protrusions. The adsorbed ether molecule layer shields the high local electric field of these small zinc protrusions, and thus blocking the further electrodeposition of zinc ions on these protrusions. This limits the capacity for significant growth of zinc dendrites (Fig. 12 b).

View Article Online
DOI: 10.1039/D0EE02079F

Apart from the electric field shielding effect, certain organic additive containing carboxide such as polyacrylamide (PAM) can improve zinc anode performance by regulating nucleation sites and overpotential (Fig. 12 d).[105] The PAM molecule in the electrolyte is firstly adsorbed onto copper mesh substrate, then the zinc ions were transferred to the surface by acyl groups of PAM. The electrostatic attraction between PAM molecules and zinc ions effectively increases the nucleation site and homogenizes the electric field and charge distribution at the interface. These positive effects ensure the uniform growth of zinc metal and form a smooth deposition surface. Due to the strong binding between zinc and PAM, the activation energy of zinc nucleation is reduced, and small-sized zinc deposits instead of large and disordered dendrites are more likely to be formed. XRD further demonstrates the low crystallinity and smaller size of zinc deposits, which is due to PAM inhibits zinc ion agglomeration and dendritic growth. DFT calculation shows the stronger binding energy between PAM and zinc compared with that between zinc and zinc (Fig. 12 c). So, PAM acts as a medium to uniformly transfer zinc from the electrolyte to the electrode surface, so as to ensure the homogeneous deposition of zinc in the whole deposition process. Battery tests confirm that PAM obviously improves the cycle stability in a wide range of current density from 0.2 mA cm^{-2} to 20 mA cm^{-2}. And the zinc deposit is small nanoparticles with 200 nm rather than large size zinc dendrites with 2 μm for normal electrolytes without PAM additive.

Organic molecules not only can regulate the interfacial distribution of zinc ion but also can affect the crystal growth orientation of zinc metal. Some organic molecules additives such as sodium dodecyl sulfate (SDS), polyethylene-glycol (PEG-8000), and thiourea (TU) are demonstrated to improve zinc anode by changing the crystal orientation of zinc plating and reduce corrosion (Fig. 12 f).[106] These additives can guide different zinc deposits with different crystallo-graphic orientations and surface textures. This is because these molecules can alter surface energy and thus guiding different preferred zinc crystal growth directions. For example, compared with no additive case in which the (101) has the strongest peak in XRD pattern, PEG

View Article Online
DOI: 10.1039/D0EE02079F

additive can make the (103) and (002) planes dominant, implying dendrite formation is less likely due to the crystal growth on the (103) plane is nearly horizontal with the electrode surface. So suitable molecule is vital for guiding the orientation of zinc crystal growth. In contrast, some additive such as cetyltrimethylammonium bromide (CTAB) is a bad additive because it can induce (101) plane and lessen (103) and (002) planes, thus dendrite formation for the CTAB case is very likely.

Synergy between electrolyte additives can sometimes produce desirable effects on the performance of zinc anodes. Huang *et al*. reported a highly efficient and stable zinc metal batteries based on adding thickener and homogenizer to the zinc sulfate electrolyte (Fig. 12 g, h).[107] The fumed silica (FS) as a thickening agent can immobilize water molecules and reduce free water content. The fatty methyl ester ethoxyl ester (FMEE) as a homogenizing agent can assist in the smooth deposition of zinc metal. The introduction of these two additives can simultaneously avoid the water-induced corrosion and inhibit zinc dendrite growth, resulting in enhanced electrochemical performances of zinc anode. Form the molecular viewpoint, this is because FS molecules can chemically bond with water molecules to mechanically protect the newly deposited zinc metal and weaken the corrosion and dendrite growth. At the same time, the FMEE additive is conducive to reducing the nucleation barriers of zinc deposition and achieving uniform zinc deposition. Electrochemical impedance spectroscopy and Tafel plots show that the $ZnSO_4$+FS+FMEE electrolyte system not only shows high conductivity but also has the lowest corrosion current density. The synergistic effect of FS and FMEE significantly improves the Coulombic efficiency of zinc deposition/stripping benefitted by inhibiting corrosion reaction and dendrite. Symmetric cell shows after adding thickener and homogenizer, the zinc anode delivers smaller polarization and longer cycle performance, and the morphology of zinc anode has no obvious dendrites.

Apart from introducing electrolyte additives, another useful strategy is to reduce the amount of water in the electrolyte (Fig. 13). For common aqueous electrolytes, water is excessive, and

View Article Online
DOI: 10.1039/D0EE02079F

thus unavoidably cause water-induced side reactions. Also, strong bonding between water molecules and zinc ions via coordination interaction is not beneficial for zinc deposition because of the high desolvation energy of hydrated zinc ion. It is thus a feasible route to reduce the relative water content of electrolytes, forming a water-starved electrolyte. The water-starved electrolytes can have several forms mainly in terms of water-in-salt electrolytes and quasi-solid-state electrolyte. Factually, when electrolyte concentration increases to a certain degree, the chemical environment around zinc ions in the aqueous electrolyte changed.[108] Zinc ions will show different electrochemical behaviors in these electrolytes because the solvation structure is altered due to the significantly reduced in water molecules.

Water-in-salt based electrolytes have been successfully tested for suppressing metal dendrite issues in metal secondary batteries. Several water-in-salt electrolytes have been developed for improving zinc anode performance. For example, a high-concentration electrolyte solution composed of 1 mol kg^{-1} $Zn(TFSI)_2$ and 20 mol kg^{-1} LiTFSI can change the solvated structure of zinc ions and thus improving zinc anode's performance.[108] In this electrolyte, a novel compact ion pair of $Zn\text{-}TFSI^+$ structure is formed because a large number of $TFSI^-$ anions migrate to the surrounding of zinc ions (Fig. 13a). This specific solution environment significantly changes the traditional hydration coordination structure of zinc ions, i.e. $Zn\text{-}(H_2O)_6)^{2+}$. This solvated structure effectively prevents HER and achieves a highly reversible (near 100% of Coulombic efficiency), dendrite-free zinc metal deposition/stripping effect (Fig. 13b). Similar to this water-in-salt electrolyte, another high concentration electrolyte called "water-in-deep eutectic solvent" electrolytes is developed.[109] This electrolyte is composed of a small amount of water (~ 30 mol %) and a eutectic mixture of urea/LiTFSI/$Zn(TFSI)_2$, which can also ensure stable and reversible zinc deposition/stripping process. In this electrolyte, the limited amount of water molecules all participate in the internal interactions with the low-eutectic materials via hydrogen bonds and coordination, leading to no-free water molecules in

View Article Online
DOI: 10.1039/D0EE02079F

the electrolyte. As a result, possible side reactions between zinc metal and free-water are significantly reduced. Battery test confirms that this high concentration electrolyte can increase the cycle life of the zinc metal deposition/stripping process by more than 20 times compared to the traditional water-heavy electrolytes.

Although the two kinds of electrolytes are satisfactory in improving battery performances, these TFSI based zinc salts are too expensive which could weaken their practical applications. So, it is a better route to prepare water-in-salt electrolytes using low-cost zinc salt. $ZnCl_2$, a common zinc salt, has high solubility which can be used to construct a high-concentration electrolyte. The as-reported high-concentration (up to 30 M) $ZnCl_2$ solution can be used as a water-in-salt electrolyte to achieve highly reversible zinc deposition/stripping.[110] In the water-starved electrolyte, hydrolysis of zinc ions can be inhibited and thus lessen the formation of passivation products such as $Zn(OH)_2$/ZnO. In contrast, these byproducts are obviously presented in low-concentration electrolytes such as 5 M of $ZnCl_2$ solution. The binding states of zinc ions in varied concentration electrolytes ranging from 5 to 30 M were studied by femtosecond excited Raman spectra, which shown that the solvated structure of zinc ion gradually transitioned from $[Zn(OH_2)_6]^{2+}$ to $[ZnCl_4]^{2-}$ (Fig. 13c). And the linear scanning voltammetry shows the broadened electrochemical stability window of $ZnCl_2$ electrolytes from 1.6 V to 2.3 V as the concentration increases from 5 to 30 M (Fig. 13d). The reshaped solvated structure of zinc ions in enough high concentration electrolyte ensures zinc anode the high reversibility of zinc plating/stripping, long cycling life and smooth deposition morphology (Fig. 13e, f).

A gel-based quasi-solid electrolyte rather than liquid phase electrolyte is also an effective route for enhancing the zinc anode performance by further weaken the water influence on zinc anode. Han *et al*. designed gelatin based Zn^{2+}-conducting solid-state electrolyte to effectively inhibit the corrosion/passivation reaction and improve the cycling performance of zinc anode.[111] The gelatin solid electrolyte (GSE) was obtained by rapidly cooling the gelatin solution to

View Article Online
DOI: 10.1039/D0EE02079F

promote random dispersion of gelatin molecules and then form a helical structure through hydrogen bond interaction. Finally, molecular interactions within the gel are further enhanced by inorganic salt via the soaking method to increase mechanical strength and simultaneously reduce water content (Fig. 13g, h). The inorganic salt can enhance the physical properties of GSE. Inorganic salt can alter the swelling/contraction behavior of GSE. GSE will swell when the salt concentration is 1M, while GSE shrinks when the salt concentration exceeds 1.5 M. The shrinkage of GSE results in dehydration which can reduce water content in GSE, and simultaneously enhance the mechanical strength of the GSE. GSE-2.5 is a better electrolyte because it has excellent mechanical strength, thermal stability and ionic conductivity simultaneously. The tensile strength of GSE-2.5 is higher than other quasi-solid-state electrolytes reported in literature, and this strong mechanical property is helpful for inhibiting zinc dendrite. Symmetric cell shows that the GSE-0 system shows large polarization and occurs short circuit after only 100 h. However, the GSE-2.5 system shows the long cycling life up to 400 h at 5 mA cm^{-2} and 2.5 mAh cm^{-2}. The morphology of zinc anode in the GSE-0 system changed significantly after cycling and accompany with the generation of by-products. In contrast, the zinc anode in the GSE-2.5 system shows stable surface morphology during plating/stripping processes (Fig. 13 i, j). The full battery of Zn-MnO_2 in this electrolyte show enhanced electrochemical reversibility and cycling performance. This enhanced performance is because GSE-2.5 has a much lower free water content than GSE-0, and thus reducing the side effects between the water and the electrode. At the same time, the GSE-2.5 has high mechanical strength, which can inhibit the dendrite growth of the zinc metal and promote the cycling performance of the full battery. Because of the flexible electrolyte of GSE-2.5, flexible full cells can well work at various extreme conditions including cutting, soaking, bending, hammering and drilling, implying multifunctionalities of the quasi-solid-state electrolyte.

3.4 Multifunctional separator designs

The separator as a vital component also play an important role on zinc plating/stripping behavior and battery performance. Common separators such as glass fiber or filter paper cannot regulate ion transport behavior. These nonselective membranes could cause a concentration gradient near zinc anode, which is a key reason for zinc dendrite growth. So, constructing multifunctional separator is an effective route to improve zinc anode. Lee *et al*. designed a robust cationic selective transport membrane as a multifunctional separator to improve the performance of zinc anode by adjusting the ion transport in the electrolyte and simultaneously as a physical barrier toward zinc dendrite (Fig. 14a-f).[115] The selective membrane (PAN-S membrane) is prepared by reaction of Li_2S_3 and PAN to firstly form a crosslinked structure with sulfur- containing functional groups, and then hydrolysis. The PAN-based ionic exchange hydrated membrane contains a large amount of water (72.4 wt%) and shows high mechanical strength with Young's modulus of 391.1 MPa, about 9 times higher than that of Nafion membrane (43.8 MPa). Ionic transport test shows the PAN-based ionic exchange hydrated membrane can selectively and effectively transport cations but blocks anions. The symmetric cell test shows the remarkably reduced voltage hysteresis (< 40 mV) and prolonged cycling life (350 cycles) of zinc deposition/stripping in the PAN-S membrane system. And the morphology of zinc plating is smooth in the PAN-S membrane system, while obvious zinc dendrites appear for ordinary separator because their large pores structure will cause uniformed zinc ion flux as expected.

A certain functional separator, may also cause the growth orientation of zinc deposits with similar to epitaxial deposition process guided by graphene. Yuan *et al.* reported a lignin@Nafion composite membrane can act as a functional separator to induce dendrite free deposition of zinc metal (Fig. 14g-j). [116] For aqueous ZIBs, it is a common phenomenon that a solid-electrolyte interface (SEI) composed of zinc hydroxide sulfate ($ZnSO_4 \cdot [Zn(OH)_2]_3 \cdot xH_2O$, denoted as ZHS) can easily form on zinc surface in near-neutral electrolytes such as aqueous $ZnSO_4$ electrolyte. Battery separators could affect the morphology of the SEI layer.

View Article Online
DOI: 10.1039/D0EE02079F

For constructing more conduction channels in Nafion and simultaneously achieving low-cost Nafion-based separators, biomass waste lignin with rich -OH groups are introduced into Nafion forming lignin@Nafion composited membranes (Fig. 14g, h). They found when compared with the common separators such as filter paper and glassy fiber, Nafion-based membranes can not only optimize the polarization and the cycling stability, but also can direct the planar ZHS layer formation. This is because the specific functional groups such as $-SO_3^-$ in Nafion can effectively coordinate with zinc ions, guiding plating/stripping behavior, leading preferred Zn (002) growth. The planar zinc (002) growth mode greatly reduces the possibility of dendrite deposition and serves as a template for ZHS growth (Fig. 14 i, j). In contrast, Zn (100) growth modes and protruded ZHS present for common filter paper separator, further demonstrating the Zn^{2+}-integrated Nafion composite membrane enable dendrite-free zinc deposition.

Directly modifying commercial glass fiber separator is another strategy to improve zinc anode performance. Li *et al*. developed a Janus separator via in situ modify vertical graphene (VG) on one side of commercial glass fiber separator by plasma enhanced chemical vapor deposition technique, [117] forming 3D VG scaffold (Figure 15 a-c). The zincophilic 3D VG conductive networks not only can homogenize electric field distribution but also lower local current density at interface (Figure 15 d-i). These merits are helpful for uniform Zn ionic flux and smooth Zn deposits. The symmetric cell based on the Janus separator can stably cycle for 600 h under a high current density of 10 mA cm^{-2} and 1 mAh cm^{-2} (Figure 15 j). One advantage of the VG modified separator is that it shows almost no decrease of the energy density for the entire device since the VG's ultrathin and ultralight feature (0.05 mg cm^{-2}). This approach is better than those coating strategies as the thick coating layers could increase obvious additional mass/volume of the entire device.

4. Conclusions and perspective

Based on the above analysis, a number of methods to optimize the performance of zinc anode depending on adequate materials and structural modification techniques were developed. However, in the face of future applications of these zinc anodes, several problems and challenges still need to be addressed. They mainly include: (1) the behavior of electrodeposition and zinc anode mechanisms in nearly neutral electrolyte at atomic or molecular levels are partially unclear; (2) practical materials and techniques must be systematically investigated to improve zinc anode commercialization; (3) further improvement is required for the zinc anode performance at high depth of discharge and its corresponding full batteries.

4.1 Electrodeposition behavior and mechanisms of zinc anode

A further study is required to understand the electrothermal behavior of zinc surface at the molecular level and to establish a desired zinc anode in the process of deposition, and related mechanism. Although zinc chemistry in alkali aqueous solution has been studied a lot, the surface chemistry on the zinc anode in near-neutral electrolyte still remains challenges. Taking into account the fact that specific electrolytes have the various chemical environments that can affect deposition mechanisms. Thus, it is necessary to understand the chemistry of zinc anode especially in the near-neutral liquid environment so as to achieve high reversibility zinc anode. For example, whether the striping/plating process of zinc in quasi-neutral solution environment has the same mechanism with the case in the acidic condition which is identified as a two-step process of gradually lossing/obtaining two electrons.[118] In addition, the detailed mechanism of side-reactions such as HER, corrosion must also be studied in view of the various pH media and salt-types that could have impact on the individual transformation processes. So far, there is no systematic report on the detailed process including rate-determining step, composition/structure of intermediates, the structure of water/oxygen at interface and their effects on the nucleation process of zinc metal.

Apart from analysing series of electochemical reaction mechanisms, deposition morphology should also be further explored. Zinc electrodeposition typically has distinct morphologies. As

View Article Online
DOI: 10.1039/D0EE02079F

mentioned above, although different methods can all improve zinc anode, and suppressing zinc dendrite morphology, those optimized zinc deposition morphologies show various models such as array type,[66] fine nanoparticle type, [68, 82] thin-film type,[49] round edge type.[77] This means zinc deposition is complicated because of many influential factors including applied voltage, current density, electrolyte types and concentration, physicochemical properties of the zinc electrode surface. In fact, the electrode surface is not static in shape during electrochemical processes. It is dynamic because of the evolution of electrode-electrolyte interface including phase and morphological changes during electrode plating and stripping processes. So, the further deep study on zinc deposition mophologies based on advanced simulation techniques will be directly beneficial for understanding interface issue and finding corresponding methods. As an effective theory for studying morphological evolution, phase-field models help explain the science behind the zinc deposition processes during cycling of ZIBs. So it is necessary to further develop the phase-field models. Lately, Hong *et al*. combine phase-field simulations with mechanical equilibrium equation to study the inuence of the mechanical property/porosity of the porous polymer/aqueous $ZnSO_4$ solution mixed electrolyte system on the dendrite growth (Fig. 16).[119] This interdisciplinary study is indeed very helpful in developing the zinc anode system with an obvious dendrite reduction effect.

4.2 Materials and techniques facing commercialization

Considering the future commercialization of ZIBs, the low-cost materials and techniques that can be used for industrialization should be more focused on and developed. Although some materials and technologies are successful in the effective control of zinc dendrite and side reactions, they cannot be readily applied in practice. This would raise the cost of building ZIB devices that do not conform with the original low-cost merit of ZIBs and do not have a reasonable implementation benefit for the modification. For potential applications it is therefore important to consider the easily available design of a low-cost but high-performance zinc anode.

Such advanced methods can aid in all zinc-based battery applications including zinc air, zinc metal and ZIB.

Different techniques such as electrodeposition, metallurgical technology, calendaring, spin coating, drop-casting and atomic layer deposition have been developed for the preparing of several enhanced zinc anodes, such as 3D-structured zinc composite and surface-modified zinc plates. Some of them have potential industrial application. Zinc foil is widely used in industry and battery fields. It has clear benefits, even so, like simple modifications to the surface chemistry of the zinc anode protective layer. However, surface coating layers tend to be imperfect with zinc-matrix, and therefore they have the possibility of being stripped away in an ongoing process of stripping/plating. In some cases, zinc deposition below the coating layer inevitably reduces coating layer adhesive with a zinc substrate that can degrade the protective effect. Besides zinc foil, zinc metal powder is an alternative to the scalable preparation of the zinc anode counterpart as an industrialized product. Considering zinc powder has a low melting temperature of about 420 ^{o}C, so zinc powder show promise to prepare 3D composite zinc anode materials with compact combination features and will be a desirable choice to improve zinc anode performances.

In addition, electrolyte developments have great success in designing practical techniques, because it is technically easy to add additives or produce water-starved electrolytes. The cycling performances on the basis of the change in electrolyte components can be compared to those on modified zinc foils, which are also expected to influence the interfacial chemistry between zinc anode and electrolytes. One of the greatest concerns with electrolyte modifications is resolving water-causing side reactions and maintaining the benefits of aqueous electrolytes, including green, safe and high ion conductivity. On the other hand, although few works focus on the modification of separator at this time , the design of dendrite-free zinc anodes may be insightful, because multifunctional separators not only induce homogenous ion transmission for uniform zinc deposition, but also cause an epitaxial-like deposition by direct

View Article Online
DOI: 10.1039/D0EE02079F

interaction between the functional group in separator and zinc ions. To promote the practical application of high-performance zinc anode, the development of scalable multifunctional separator syntheses techniques will be quite helpful.

Zinc dendrite formation, as described in Fig. 2, becomes more severe at large areal capacity during homogenous nucleation. This may prevent highly efficient zinc anode from being implemented. Due to its zinc deposit structures, the induction of epitaxial anodes may be the better way to build a high-performance anode for large area capacity. Epitaxial zinc anode induced by graphene can still show high efficiencies even with high rates and current density as shown in Fig. 11. The viability of the epitaxial zinc anode induced by graphene therefore deserves further discussion. Although graphene material can induce epitaxial electrodeposition of zinc, some key problems and contradictory facts are not clear. For instance, the kinetic process for zinc deposition on graphene surface was not investigated systematically. And although epitaxial zinc structure can be formed based on the small lattice matching criterion between graphene and zinc, the low zincophilicity of graphene with zinc ions implies that graphene substrate is unfavorable for zinc deposition.[105] Additionally, graphene shows variety primarily caused by various methods of preparation.[120, 121] A consistency measures for graphene products by more than sixty world graphene manufacturers show this.[121] These graphene samples are clearly distinct in terms of purity, lattice defects, thickness (layers), and lateral dimensions. As a consequence, there are several uncertainties for making the graphene substrate that is ideal for inducing epitaxial growth on zinc anode. So, it should also be made clear that the relationship between graphene and epitaxial zinc anode parameters, which may provide the most relevant technology reference for preparing the functional graphene substrate.

Most importantly, how to construct a macroscopic ordered graphene layer structure that can be used as a substrate for epitaxial zinc anode in practice. At present, the reported oriented graphene substrate is coated on the stainless-steel plate by applying rheological properties of graphene dispersion.[49] However, because of the extra mass of the stainless-steel plate the

View Article Online
DOI: 10.1039/D0EE02079F

graphene/stainless-steel electrode is not in use in operating condition. Thus, free-standing graphene film as a substrate will be more favorable for practical usage. Apart from taking advantage of the rheological properties of graphene solutions, other solution properties of graphene dispersion can also be considered to construct oriented graphene films. In fact, graphene materials have excellent dispersibility in liquids, and the resulting graphene dispersion shows a variety of solution chemical properties, including colloidal properties, rheological properties, self-assembly properties, liquid crystal properties, which can provide possibility for assembling graphene sheets to macroscopic ordered graphene structure for practical epitaxial zinc anode.

4.3 Discharge depth study of zinc anode

Full battery experiments have shown improved battery efficiency based on modified zinc anode structures that match a range of cathode materials such as manganese oxide and vanadium oxide. Especially, a certain simple method can obviously enhance cycling stability of full battery such as Zn-MnO_2 battery (Fig. 17), which is instructive for constructing practical ZIBs. In the meantime, it should be noted that most methods developed at present only studied the performance of zinc anodes at a low areal capacity and discharge depth.[41] Although prolonged cycle lifetime (>3000 h) can be obtained by modifying zinc anode, the Zn plating/stripping capacities are generally low (less than 1 mAh cm^{-2}).[68, 77, 82, 112] This is not beneficial for assembling practical full batteries especially with high mass loading of cathode materials. It therefore requires electrochemical performances of modified anode in a high degree of discharge, which can achieve desirable result at large deposition areal capacity and with high mass loading of matched cathode material in a practical full battery system. In the use of planar zinc anode, the thickness of the zinc foil/plate is a significant parameter. Most of the currently used zinc foil/plate are too thick (100-250 μm), which is not beneficial for assembly practical full battery with low negative/positive capacity ratio (N:P). The relationship of thickness/depth of discharge of the zinc foil with the battery performance needs therefore to

View Article Online
DOI: 10.1039/D0EE02079F

be studied. Different forms of zinc anode such as zinc foil, porous zinc, zinc powder and specific substrate supported zinc anode (Fig. 18) can be further studied to obtain ideal battery performance under high depth of discharge.

In short, a set of materials and the related structures were designed to enhance the zinc plating/stripping behavior and thus the cycling stability and rates efficiency of the battery. Such materials and structures are based primarily on the development of two effects namely the homogeneous deposition and epitaxial deposition of zinc metal via many ways in response to electron and ion behavior. All of these routes can prevent the evident growth of dendrite, forming dendrite-free zinc deposit. The continuous production of new functional materials on the basis of micron-, nano- or molecular-level materials and rationally constructed structures gives the development of ideal zinc anode and ZIBs future applications great importance. Electrodeposition of metals has some similarities, so studying zinc electrodeposition to optimize electrochemical performances of a zinc anode and related full batteries is helpful for both zinc-based batteries as well as other metal-based secondary batteries.

Acknowledgements

This research work was financially supported by the National Natural Science Foundation of China (Grant. Nos. 51771058, 11474047, 51801030), Pearl River Talent Program of Guangdong Province (2017GC010030), Guangdong Province Universities and Colleges Pearl River Scholar Funded Scheme, Natural Science Foundation of Guangdong Providence (Grant No. 2018A030310571), One-hundred Young Talents (Class A) of Guangdong University of Technology (Grant No. 220413198).

References

1 N. Kittner, F. Lill and D.M. Kammen, *Nat. Energy*, 2017, **2**, 17125.

2 B. Obama, *Science*, 2017, **355**, 126–129.

3 W. Lee, S. Muhammad, C. Sergey, H. Lee, J. Yoon,Y. Kang and W. Yoon, *Angew. Chem. Int. Ed*., 2020, **59**, 2578–2605.

4 E.C. Evarts, *Nature*, 2015, **526**, S93–S95.

5 J.B. Goodenough, *Nat. Electron.*, 2018, **1**, 204.

6 R. J. Clément, Z. Lun and G. Ceder, *Energy Environ. Sci.,* 2020,**13**, 345–373.

7 A. M. Haregewoin, A. S. Wotango and B. Hwang, *Energy Environ. Sci*., 2016,**9**, 1955–1988.

8 D. Chao, W. Zhou, F. Xie, C. Ye, H. Li, M. Jaroniec and S. Qiao, *Sci. Adv*., 2020, **6**, eaba4098.

9 R. Rajagopalan, Y. Tang, C. Jia, X. Ji and H. Wang, *Energy Environ. Sci.,* 2020,**13**, 1568–1592.

10 F. Wang, X. Wu, C. Li, Y. Zhu, L. Fu, Y. Wu and X. Liu, *Energy Environ. Sci.*, 2016,**9**, 3570–3611.

11 H. Kim, J. Hong, K. Park, H. Kim, S. Kim and K. Kang, *Chem. Rev.,* 2014, **114**, 11788–11827.

12 A.L. Lipson, B. Pan, S.H. Lapidus, C. Liao, J.T. Vaughey and B.J. Ingram, *Chem. Mater.,* 2015, **27**, 8442–8447.

13 H. D. Yoo, I. Shterenberg, Y. Gofer, G. Gershinsky, N. Pour and Doron Aurbach, *Energy Environ. Sci*., 2013,**6**, 2265–2279.

14 L.E. Blanc, D. Kundu and L.F. Nazar, *Joule,* 2020, **4**, 771–799.

15 G. Fang, J. Zhou, A. Pan and S. Liang, *ACS Energy Lett.,* 2018, **3**, 2480–2501.

16 A. Konarov, N. Voronina, J.H. Jo, Z. Bakenov, Y. Sun and S. Myung, *ACS Energy Lett.,* 2018, **3**, 2620–2640.

17 J. Ming, J. Guo, C. Xia, W. Wang and H.N. Alshareef, *Mat. Sci. Eng. R.,* 2019, **135**, 58–84.

18 D. Selvakumaran, A. Pan, S. Liang and G. Cao, *J. Mater. Chem. A,* 2019, **7**, 18209–18236.

19 M.H. Askar, H. Abbas and S.E. Afifi, *J. Power Sources,* 1994, **48**, 303–309.

20 Y. Li, M. Gong, Y. Liang, J. Feng, J. Kim, H. Wang, G. Hong, B. Zhang and H. Dai, *Nat. Commun.,* 2013, **4**, 1805.

21 A.R. Mainar, O. Leonet, M. Bengoechea, I. Boyano, I. De Meatza, A. Kvasha, A. Guerfi and J.A. Blazquez, *Int. J. Energ. Res.,* 2016, **40**, 1032–1049.

22 J. McBreen, *J. Power Sources,* 1994, **51**, 37–44.

23 D.F. Smith and J.A. Gucinski, *J. Power Sources,* 1999, **80**, 66–71.

24 D. Boden, C.J. Venuto, D. Wisler and R.B. Wylie, *J. Electrochem. Soc.,* 1967, **115**, 333–338.

25 H.Y. Kang and C.C. Liang, *J. Electrochem. Soc.,* 1968, **115**, 6–10.

26 T. Shoji, M. Hishinuma and T. Yamamoto, *J. Appl. Electrochem.,* 1988, **18**, 521–526.

27 T. Yamamoto and T. Shoji, *Inorg. Chim. Acta,* 1986, **117**, L27–L28.

28 C. Xu, B. Li, H. Du and F. Kang, *Angew. Chem., Int. Ed.,* 2012, **51**, 933–935.

29 B. Wu, G. Zhang, M. Yan, T. Xiong, P. He, L. He, X. Xu and L. Mai, *Small,* 2018, **14**, 1703850.

30 N. Zhang, F. Cheng, J. Liu, L. Wang, X. Long, X. Liu, F. Li and J. Chen, *Nat. Commun.*, 2017, **8**, 405.

31 J. Huang, Z. Wang, M. Hou, X. Dong, Y. Liu, Y. Wang and Y. Xia, *Nat. Commun.*, 2018, **9**, 2906.

32 S. Liu, H. Zhu, B. Zhang, G. Li, H. Zhu, Y. Ren, H. Geng, Y. Yang, Q. Liu and C. C. Li, *Adv. Mater.* 2020, 2001113.

33 H. Geng, M. Cheng, B. Wang, Y. Yang, Y. Zhang and C. C. Li, *Adv. Funct. Mater.,* 2020, **30**, 1907684.

34 Q. Zhao, W. Huang, Z. Luo, L. Liu, Y. Lu, Y. Li, L. Li, J. Hu, H. Ma and J. Chen, *Sci. Adv.,* 2018, **4**, eaao1761.

35 D. Kundu, P. Oberholzer, C. Glaros, A. Bouzid, E. Tervoort, A. Pasquarello and M. Niederberger, *Chem. Mater.*, 2018, **30**, 3874–3881.

36 W. Du, H. Geng, Y. Yang, Y. Zhang, H. Ang, M. Ye and C. C. Li, *J. Power Sources*, 2020, **450**, 227716.

37 C. Han, W. Li, H.K. Liu, S. Dou and J. Wang, *Nano Energy,* 2020, **74**, 104880.

38 H. Jia, Z. Wang, B. Tawiah, Y. Wang, C. Chan, B. Fei and F. Pan, *Nano Energy,* 2020, **70**, 104523.

39 C. Li, X. Xie, S. Liang and J. Zhou, *Energy Environ. Mater.,* 2020, **0**,1–14,

40 Y. Yu, W. Xu, X. Liu and X. Lu, *Adv. Sustainable Syst.* 2020, 2000082.

41 J. Shin, J.M. Lee, Y. Park and J.W. Choi, *Chem. Sci.,* 2020, **11**, 2028–2044.

42 B. Tang, L. Shan, S. Liang and J. Zhou, *Energy Environ. Sci.,* 2019, **12**, 3288–3304.

43 K. Wang, *ACS Omega,* 2020, **5**, 10225–10227.

44 T.H. Wu, Y. Zhang, Z.D. Althouse and N. Liu, *Mater. Today Nano,* 2019, **6**, 100032.

45 P. Yu, Y. Zeng, H. Zhang, M. Yu, Y. Tong and X. Lu, *Small* 2019, **15**, 1804760.

46 Q. Zhang, J. Luan, Y. Tang, X. Ji and H. Wang, *Angew. Chem. Int. Ed*., 2020, **59**, 2–14.

47 Y. Zhang, Z. Chen, H. Qiu, W. Yang, Z. Zhao, J. Zhao and G. Cui, *NPG Asia Mater.,* 2020, **12**, 1–24.

48 Z. Cao, P. Zhuang, X. Zhang, M. Ye, J. Shen and P. M. Ajayan, *Adv. Energy Mater*., 2020, 2001599.

49 J. Zheng, Q. Zhao, T. Tang, J. Yin, C.D. Quilty, G.D. Renderos, X. Liu, Y. Deng, L. Wang and D.C. Bock, *Science*, 2019, **366**, 645–648.

50 L. Su, L. Liu, B. Liu, J. Meng and X. Yan, *iScience*, 2020, **23**, 100995.

51 L. Liang, Y. Qi, F. Xue, S. Bhattacharya, S.J. Harris and L. Chen, *Phys. Rev. E,* 2012, **86**, 051609.

View Article Online
DOI: 10.1039/D0EE02079F

52 D.A. Cogswell, *Phys. Rev. E,* 2015, **92**, 011301.

53 S.Y. Pan and M.F. Zhu, *IOP Conf. Ser.: Mater. Sci. Eng.,* 2012, **33**, 012096.

54 T.N. Ostanina, V.M. Rudoi, V.S. Nikitin, A.B. Darintseva, O.L. Zalesova and N.M. Porotnikova, *Russ. J. Non-Ferr. Met.,* 2016, **57**, 47–51.

55 Y. Shibuta, Y. Okajima and T. Suzuki, *Sci.Technol. Adv. Mat.,* 2007, **8**, 511–518.

56 J.E. Guyer, W.J. Boettinger, J.A. Warren and G. B. Mcfadden, *Phys. Rev. E,* 2004, **69**, 021604.

57 J.E. Guyer, W.J. Boettinger, J.A. Warren and G.B. Mcfadden, *Phys. Rev. E,* 2004, **69**, 021603.

58 D. C. Grahame, *Chem. Rev.*, 1947, **41**, 441–501.

59 F. Sagues, M.Q. Lopezsalvans and J. Claret, *Phys. Rep.,* 2000, **337**, 97–115.

60 A. Karma and W. Rappel, *Phys. Rev. E,* 1998, 57, 4323–4349.

61 C. Chen and J. Jorne, *Journal. Electrochem. Soc.,* 1990, **137**, 2047–2051.

62 Y. Sawada, A. Dougherty and J.P. Gollub, *Phys. Rev. Lett.,* 1986, **56**, 1260–1263.

63 M. Matsushita, M. Sano, Y. Hayakawa, H. Honjo and Y. Sawada, *Phys. Rev. Lett.,* 1984, **53**, 286–289.

64 Q. Yang, G. Liang, Y. Guo, Z. Liu, B. Yan, D. Wang, Z. Huang, X. Li, J. Fan and C. Zhi, *Adv. Mater.,* 2019, **31**, 1903778.

65 J. Kasemchainan, S. Zekoll, D.S. Jolly, Z. Ning, G.O. Hartley, J. Marrow and P.G. Bruce, *Nat. Mater.,* 2019, **18**, 1105–1111.

66 M. Cui, Y. Xiao, L. Kang, W. Du, Y. Gao, X. Sun, Y. Zhou, X. Li, H. Li, F. Jiang and C. Zhi, *ACS Appl. Energy Mater.,* 2019, **2**, 6490–6496.

67 D. Han, S. Wu, S. Zhang, Y. Deng, C. Cui, L. Zhang, Y. Long, H. Li, Y. Tao, Z. Weng, Q. Yang and F. Kang, *Small,* 2020, 2001736.

68 P. Liang, J. Yi, X. Liu, K. Wu, Z. Wang, J. Cui, Y. Liu, Y. Wang, Y. Xia and J. Zhang, *Adv. Funct. Mater.,* 2020, **30**, 1908528.

69 K. Zhao, C. Wang, Y. Yu, M. Yan, Q. Wei, P. He, Y. Dong, Z. Zhang, X. Wang and L. Mai, *Adv. Mater. Interfaces* 2018, **5**, 1800848.

70 H. He, H. Tong, X. Song, X. Song and J. Liu, *J. Mater. Chem. A,* 2020, **8**, 7836–7846.

71 X. Xie, S. Liang, J. Gao, S. Guo, J. Guo, C. Wang, G. Xu, X. Wu, G. Chen and J. Zhou, *Energy Environ. Sci*., 2020, **13**, 503–510.

72 J. Y. Kim, G. Liu, G. Y. Shim, H. Kim and J. K. Lee, *Adv. Funct. Mater*., 2020, 2004210.

73 J. Hao, B. Li, X. Li, X. Zeng, S. Zhang, F. Yang, S. Liu, D. Li, C. Wu and Z. Guo, *Adv. Mater.,* 2020, 2003021.

74 L. Kang, M. Cui, F. Jiang, Y. Gao, H. Luo, J. Liu, W. Liang and C. Zhi, *Adv. Energy Mater.,* 2018, **8**, 1801090.

75 C. Deng, X. Xie, J. Han, Y. Tang, J. Gao, C. Liu, X. Shi, J. Zhou and S. Liang, *Adv. Funct. Mater.,* 2020, **30**, 2000599.

76 R. Yuksel, O. Buyukcakir, W.K. Seong and R.S. Ruoff, *Adv. Energy Mater.,* 2020, **10**, 1904215.

77 H. Yang, Z. Chang, Y. Qiao, H. Deng, X. Mu, P. He and H. Zhou, *Angew. Chem. Int. Ed*., 2020, **59**, 9377–9381.

78 Z. Zhou, Y. Zhang, P. Chen, Y. Wu, H. Yang, H. Ding, Y. Zhang, Z. Wang, X. Du and N. Liu, *Chem. Eng. Sci.,* 2019, **194**, 142–147.

79 C. Shen, X. Li, N. Li, K.Xie, J. Wang, X. Liu and B. Wei, *ACS Appl. Mater. Interfaces*, 2018, **10**, 25446–25453.

80 A. Wang, W. Zhou, A. Huang, M. Chen, J. Chen, Q. Tian and J. Xu, *J. Colloid Interf. Sci.,* 2020, **577**, 256–264.

81 Q. Yang, Y. Guo, B. Yan, C. Wang, Z. Liu, Z. Huang, Y. Wang, Y. Li, H. Li, L. Song, J. Fan and C. Zhi, *Adv. Mater.,* 2020, **32**, 2001755.

82 Z. Zhao, J. Zhao, Z. Hu, J. Li, J. Li, Y. Zhang, C. Wang and G. Cui, *Energy Environ. Sci*., 2019, **12**, 1938–1949.

83 J. Hao, X. Li, S. Zhang, F. Yang, X. Zeng, S. Zhang, G. Bo, C. Wang and Z. Guo, *Adv. Funct. Mater.* 2020, 2001263.

84 R. Zhao, Y. Yang, G. Liu, R. Zhu, J. Huang, Z. Chen, Z. Gao, X. Chen and L. Qie, *Adv. Funct. Mater.* 2020, 2001867.

85 Y. Cui, Q. Zhao, X. Wu, X. Chen, J. Yang, Y. Wang, R. Qin, S. Ding, Y. Song, J. Wu, K. Yang, Z. Wang, Z. Mei, Z. Song, H. Wu, Z. Jiang, G. Qian, L. Yang and F. Pan, *Angew. Chem. Int. Ed*., 2020, doi: 10.1002/anie.202005472.

86 W. Guo, Z. Cong, Z. Guo, C. Chang, X. Liang, Y. Liu, W. Hu and X. Pu, *Energy Storage Materials,* 2020, **30**, 104–112.

87 J.F. Parker, C.N. Chervin, I.R. Pala, M. Machler, M.F. Burz, J.W. Long and D.R. Rolison, *Science* 2017, **356**, 415–418.

88 L. Wang, N. Li, T. Wang, Y. Yin, Y. Guo and C. Wang, *Electrochim. Acta,* 2017, **244**, 172–177.

89 W. Dong, J.-L. Shi, T.-S. Wang, Y.-X. Yin, C.-R. Wang and Y.-G. Guo, *RSC Adv.,* 2018, **8**, 19157–19163.

90 Y. Zeng, X. Zhang, R. Qin, X. Liu, P. Fang, D. Zheng, Y. Tong and X. Lu, *Adv. Mater.,* 2019, **31**, 1903675.

91 Y. Zhou, X. Wang, X. Shen, Y. Shi, C. Zhu, S. Zeng, H. Xu, P. Cao, Y. Wang, J. Di and Q. Li, *J. Mater. Chem. A,* 2020, **8**, 11719–11727.

92 Y. Yin, S. Wang, Q. Zhang, Y. Song, N. Chang, Y. Pan, H. Zhang and X. Li, *Adv. Mater.,* 2020, **32**, 1906803.

93 D. Chao, C.R. Zhu, M. Song, P. Liang, X. Zhang, N.H. Tiep, H. Zhao, J. Wang, R. Wang and H. Zhang, *Adv. Mater.,* 2018, **30**, 1803181.

94 H. Li, C. Xu, C. Han, Y. Chen, C. Wei, B. Li and F. Kang, *J. Electrochem. Soc.,* 2015, **162**, A1439–A1444.

95 Z. Wang, J. Huang, Z. Guo, X. Dong, Y. Liu, Y. Wang and Y. Xia, *Joule*, 2019, **3**, 1289–1300.

96 Y. Tian, Y. An, C. Wei, B. Xi, S. Xiong, J. Feng and Y. Qian, *ACS Nano,* 2019, **13**, 11676–11685.

97 X. Shi, G. Xu, S. Liang, C. Li, S. Guo, X. Xie, X. Ma and J. Zhou, *ACS Sustain. Chem. Eng.,* 2019, **7**, 17737–17746.

98 C. Li, X. Shi, S. Liang, X. Ma, M. Han, X. Wu and J. Zhou, *Chem. Eng. J.,* 2020, **379**, 122248.

99 J. Zhao, H. Ren, Q. Liang, D. Yuan, S. Xi, C. Wu, W. Manalastas, J. Ma, W. Fang and Y. Zheng, *Nano Energy,* 2019, **62**, 94–102.

100 Z. Kang, C. Wu, L. Dong, W. Liu, J. Mou, J. Zhang, Z. Chang, B. Jiang, G. Wang, F. Kang and C. Xu, *ACS Sustainable Chem. Eng*., 2019, **7**, 3364–3371.

101 S.-B. Wang, Q. Ran, R.-Q. Yao, H. Shi and Q. Jiang, *Nat. Commun.,* 2020, **11**, 1634.

102 B. Liu, S. Wang, Z. Wang, H. Lei and W. Mai, *Small,* 2020, **16**, 2001323.

103 Z. Cai, Y. Ou, J. Wang, R. Xiao, L. Fu, Z. Yuan, R. Zhan and Y. Sun, *Energy Storage Materials* 2020, **27**, 205–211.

104 W. Xu, K. Zhao, W. Huo, Y. Wang, G. Yao, X. Gu, H. Cheng, L. Mai, C. Hu and X. Wang, *Nano Energy,* 2019, **62**, 275–281.

105 Q. Zhang, J. Luan, L. Fu, S. Wu, Y. Tang, X. Ji and H. Wang, *Angew. Chem. Int. Ed.,* 2019, **58**, 15841–15847.

106 K.E.K. Sun, T.K.A. Hoang, Y. Yu, X. Zhu, Y. Tian and P. Chen, *ACS Appl. Mater. Inter.,* 2017, **9**, 9681–9687.

107 J. Huang, X. Chi, Q. Han, Y. Liu, Y. Du, J. Yang and Y. Liu, *J. Electrochem. Soc.,* 2019, **166**, A1211–A1216.

108 F. Wang, O. Borodin, T. Gao, X. Fan, W. Sun, F. Han, A. Faraone, J.A. Dura, K. Xu and C. Wang, *Nat. Mater.,* 2018, **17**, 543–549.

109 J. Zhao, J. Zhang, W. Yang, B. Chen, Z. Zhao, H. Qiu, S. Dong, X. Zhou, G. Cui and L. Chen, *Nano Energy*, 2019, **57**, 625–634.

110 C. Zhang, J. Holoubek, X. Wu, A. Daniyar, L. Zhu, C. Chen, D. P. Leonard, I. A. Rodríguez-Pérez, J. Jiang, C. Fang and X. Ji, *Chem. Commun.,* 2018, **54**, 14097–14099.

111 Q. Han, X. Chi, Y. Liu, L. Wang, Y. Du, Y. Ren and Y. Liu, *J. Mater. Chem. A,* 2019, **7**. 22287–22295.

112 L. Wang, Y. Zhang, H. Hu, H.-Y. Shi, Y. Song, D. Guo, X.-X. Liu and X. Sun, *ACS Appl. Mater. Inter.,* 2019, **11**, 42000–42005.

113 W. Li, K. Wang, M. Zhou, H. Zhan, S. Cheng and K. Jiang, *ACS Appl. Mater. Inter.,* 2018, **10**, 22059–22066.

114 S. Huang, F. Wan, S. Bi, J. Zhu, Z. Niu and J. Chen, *Angew. Chem. Int. Ed.* 2019, **58**, 4313–4317.

115 B. Lee, S. Cui, X. Xing, H. Liu, X. Yue, V. Petrova, H. Lim, R. Chen and P. Liu, *ACS Appl. Mater. Inter.,* 2018, **10**, 38928–38935.

116 D. Yuan, W. Manalastas, L. Zhang, J.J. Chan, S. Meng, Y. Chen and M. Srinivasan, *Chemsuschem,* 2019, **12**, 4889–4900.

117 C. Li, Z. Sun, T. Yang, L. Yu, N. Wei, Z. Tian, J. Cai, J. Lv, Y. Shao, M. H. Rümmeli, J. Sun and Z. Liu, *Adv. Mater*., 2020, 2003425.

118 L. M. Baugh, *Electrochim. Acta* 1979, **24**, 657–667.

119 Z. Hong, Z. Ahmad and V. Viswanathan, *ACS Energy Lett*., 2020, **5**, 2466–2474.

120 W. Du, H. Geng, Y. Yang, Y. Zhang, X. Rui and C. C. Li, J. Power Sources, 2019, **437**, 226899.

121 A. P. Kauling, A. T. Seefeldt, D. P. Pisoni, R. C. Pradeep, R. Bentini, R. V. B. Oliveira, K. S. Novoselov and A. H. Castro Neto, *Adv. Mater*., 2018, 1803784.

View Article Online
DOI: 10.1039/D0EE02079F

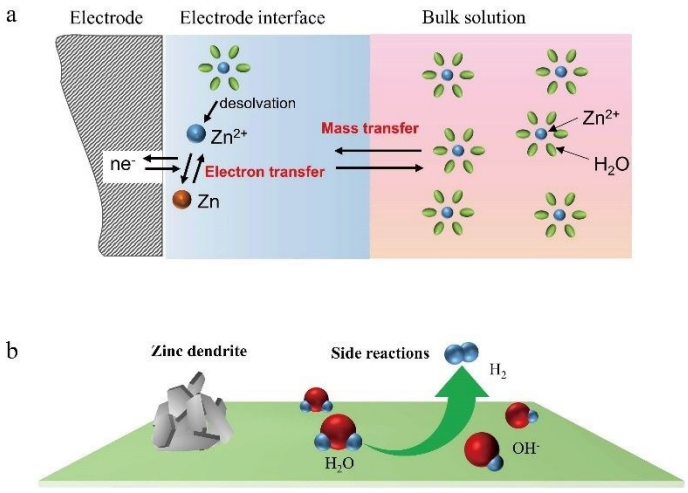

Fig. 1 (a) Schematic representation of the deposition/stripping processes of zinc anode in ZIBs (not to scale). (b) Schematic illustration of Zinc dendrite and interface side reactions of zinc anode.

View Article Online
DOI: 10.1039/D0EE02079F

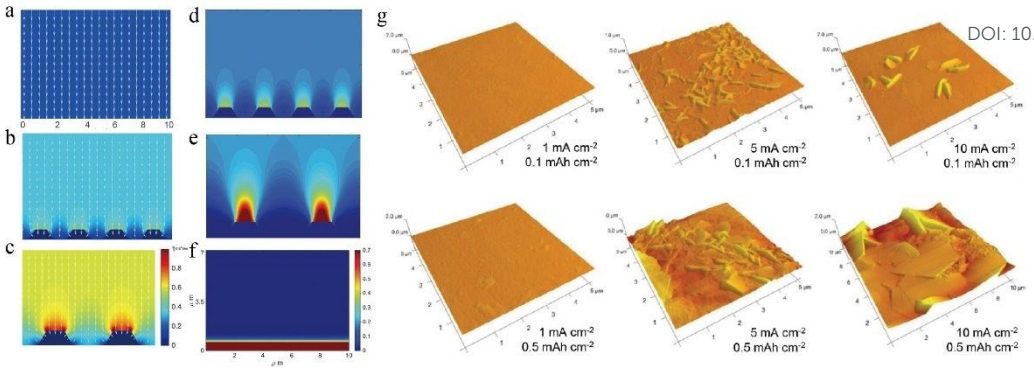

Fig. 2 (a-c) Simulation of electric field on the surface of Zn electrodes after the first charging process with 0.1 mAh cm^{-2} at different current densities of (a) 1 mA cm^{-2}, (b) 5 mA cm^{-2}, (c)10 mA cm^{-2}. (d-f) Simulation of Zn-ion diffusion and distribution along the 2D surface of electrodes with different conditions of dendrite formation: d) 4 small dendritic seeds, e) 2 large dendritic seeds, f) flat surface. (g) AFM images of Zn electrodes cycled at 1, 5, 10 mA cm^{-2} with a constant capacity of 0.1 mAh cm^{-2} and 0.5 mAh cm^{-2} to observe the nucleation behaviour at the initial stage. Reprinted with permission from ref. 64. Copyright 2019 Wiley-VCH Verlag GmbH & Co. KGaA, Weinheim.

View Article Online
DOI: 10.1039/D0EE02079F

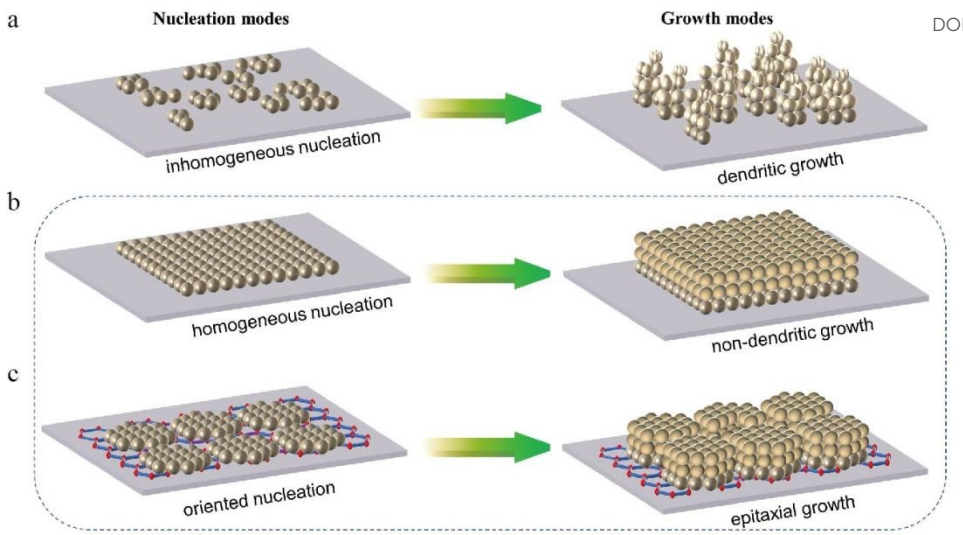

Fig. 3 (a) inhomogeneous nucleation and dendritic growth of zinc anode. Two strategies for solving dendritic problem: (b) induced homogeneous nucleation avoiding obvious dendritic growth mode, and (c) designing specific substrate induced epitaxial deposition mode.

View Article Online
DOI: 10.1039/D0EE02079F

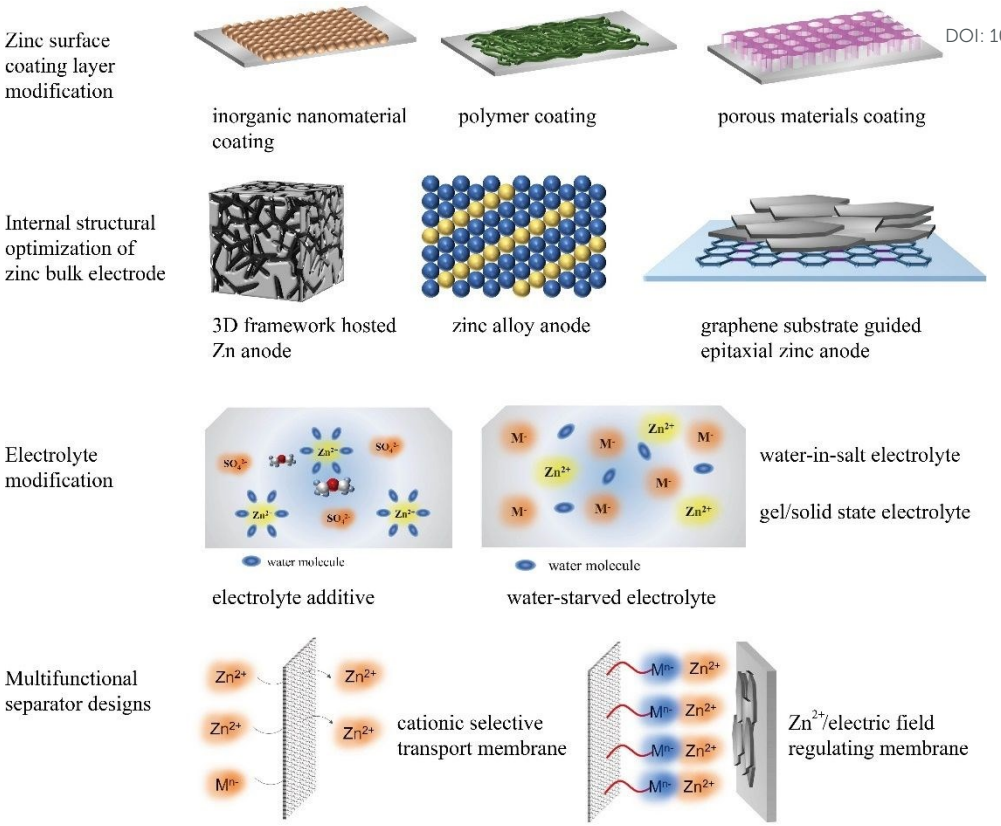

Fig. 4 General strategies for solving zinc anode problems (including dendrite and side reaction issues).

View Article Online
DOI: 10.1039/D0EE02079F

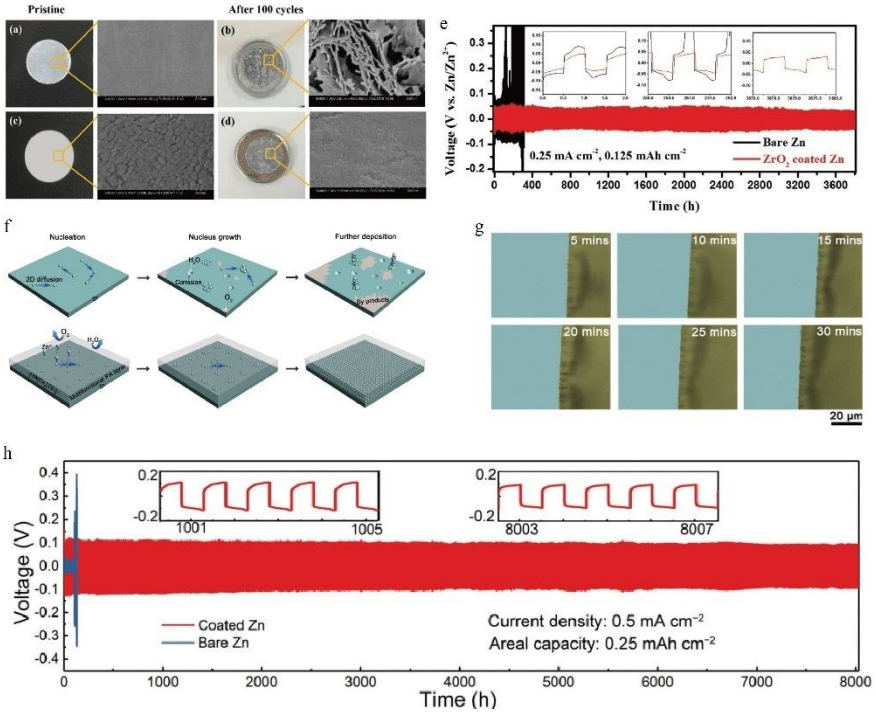

Fig. 5 Digital images and corresponding SEM images of a, b) the bare Zn anode and c, d) the ZrO_2-coated Zn anode before and after 100 cycles at 5 mA cm^{-2} with a capacity of 2.5 mAh cm^{-2}. (e) Voltage profiles of the metallic Zn plating/stripping in Zn symmetric full-cell and ZrO_2-coated Zn symmetric full-cell at 0.25 mA cm^{-2} for 0.125 mAh cm^{-2}. Reprinted with permission from ref. 68. Copyright 2020 Wiley-VCH Verlag GmbH & Co. KGaA, Weinheim. (f) Schematic diagrams for Zn deposition: the PA layer coating endows a dense and dendrite-free deposition morphology by refining the nucleus size, increasing the nucleus density resulted from constraining the 2D mass diffusion, and inhibiting the permeation of O_2 and H_2O. (g) Cross-sectional Zn deposition morphology on PA coated Zn plate in the symmetrical Zn cell at a current density of 10 mA cm^{-2} using an in situ optical microscope. (h) Long-term galvanostatic cycling of symmetrical Zn cells with coated Zn plates and bare Zn plates at a current density of 0.5 mA cm^{-2}. Reproduced from Ref. 82 with permission from The Royal Society of Chemistry.

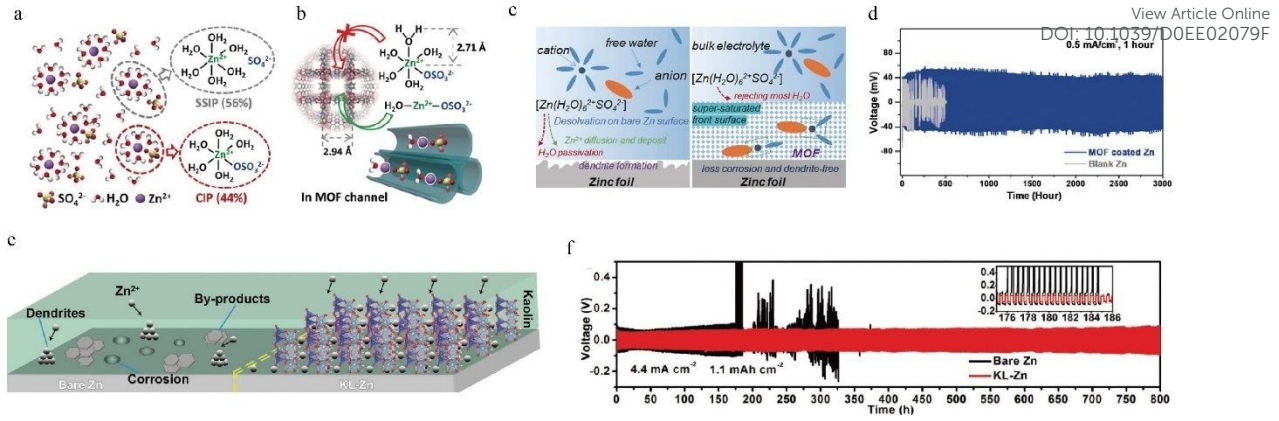

Fig. 6 (a) Two solvation structures in saturated (3.3 M) $ZnSO_4$ aqueous solutions. (b) Schematic illustration of highly-coordinated ion complexes of H_2O-Zn^{2+}-OSO_3^{2-} migrating through MOF channels. (c) schematic illustration of Zn surface evolution. left: severe water passivation and dendrite formation caused by attack from desolvation process on bare Zn foil. right: function mechanism of MOF coating layer to reject H_2O and construct a super-saturated front surface.; (d) Long-term cyclic stability of symmetric cells in 2 M $ZnSO_4$ aqueous electrolyte at current density of 0.5 mA cm^{-2} for bare Zn and MOF-coated Zn anode, respectively. Reprinted with permission from ref. 77. Copyright 2020 Wiley-VCH Verlag GmbH & Co. KGaA, Weinheim. (e) Schematic illustrations of morphology of Zn and Kaolin (KL)-Zn anodes during Zn^{2+} deposition process. (f) Long-term galvanostatic cycling results of symmetrical cells with different electrodes at 4.4 mA cm^{-2}. Reprinted with permission from ref. 75. Copyright 2020 Wiley-VCH Verlag GmbH & Co. KGaA, Weinheim.

View Article Online
DOI: 10.1039/D0EE02079F

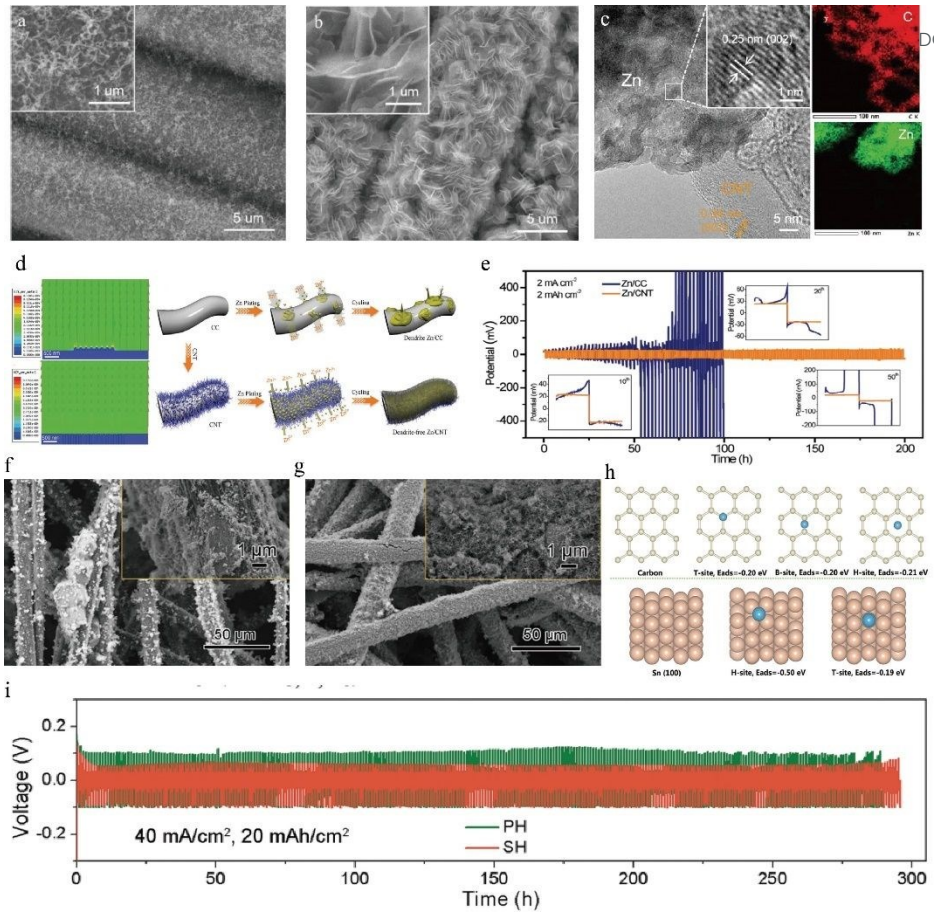

Fig. 7 SEM images of CNT (a) and Zn/CNT (b) samples. (c) high-resolution TEM images of Zn/CNT sample and selected-area elemental mapping images of C and Zn for Zn/CNT sample. (d) Models of the electric field distributions for a Zn/CC electrode and a Zn/CNT electrode after Zn nuclei formation, and the schematic illustrations of Zn deposition on CC and CNT electrodes. (e) Voltage profiles of symmetric cells based on Zn/CC and Zn/CNT anodes at 2 mA cm^{-2}. Reprinted with permission from ref. 90. Copyright 2019 Wiley-VCH Verlag GmbH & Co. KGaA, Weinheim. SEM images of f) carbon felt host (PH) and g) Sn modified 3D carbon felt host (SH) after charging (inset, higher magnification) (h) DFT calculations. Adsorption energy of carbon and Sn. (i) charge–discharge curves of in the Zn symmetrical flow batteries with PH and SH. Reprinted with permission from ref. 92. Copyright 2019 Wiley-VCH Verlag GmbH & Co. KGaA, Weinheim.

View Article Online
DOI: 10.1039/D0EE02079F

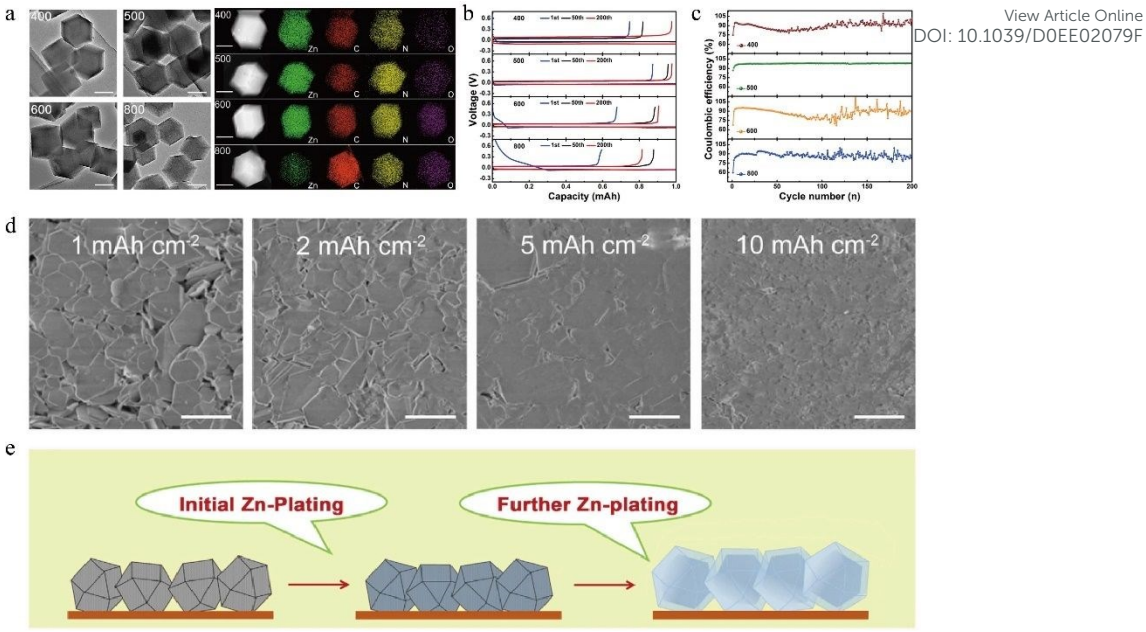

Fig. 8 (a) TEM images of the ZIF-8 samples prepared at 400 °C, 500 °C, 600 °C, and 800 °C, and corresponding elemental mappings. (b) The polarization of the plating and stripping for the different electrodes at 2.0 mA cm^{-2} with a capacity of 1.0 mAh cm^{-2}. (c) Coulombic efficiency of the plating and stripping for the different electrodes at 2.0 mA cm^{-2} with a capacity of 1.0 mAh cm^{-2}. (d) SEM images of Zn deposits at a current density of 1.0 mA cm^{-2} for different capacities. Scale bars, 2 mm. (e) Schematic illustration of the Zn plating. Reprinted with permission from ref. 95. Copyright 2019 Elsevier.

View Article Online
DOI: 10.1039/D0EE02079F

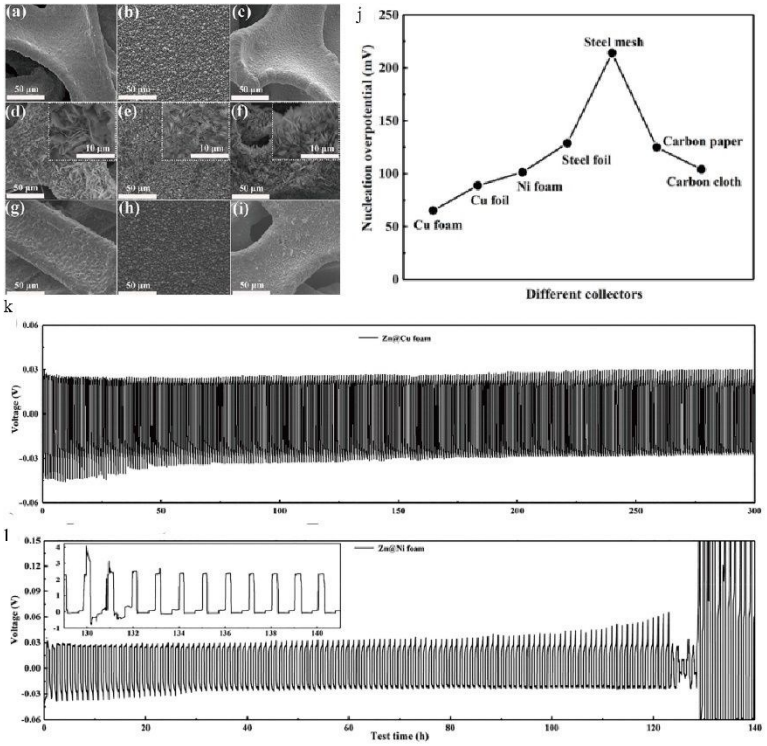

Fig.9 SEM images of (a) Cu foam, (b) Cu foil, and (c) Ni foam in the pristine state. SEM images of (d) Zn@Cu foam, (e) Zn@Cu foil, and (f) Zn@Ni foam after the plating process. SEM images of (g) Zn@Cu foam, (h) Zn@Cu foil, and (i) Zn@Ni foam after the stripping process. (j) Zn nucleation overpotentials of different collectors. (l) Voltage−time profiles of Zn@Cu foam and Zn@Ni foam symmetric cells at the current of of 2 mA cm^{-2} and an areal capacity of 1 mA h cm^{-2}. Reprinted with permission from ref. 97. Copyright 2019 American Chemical Society.

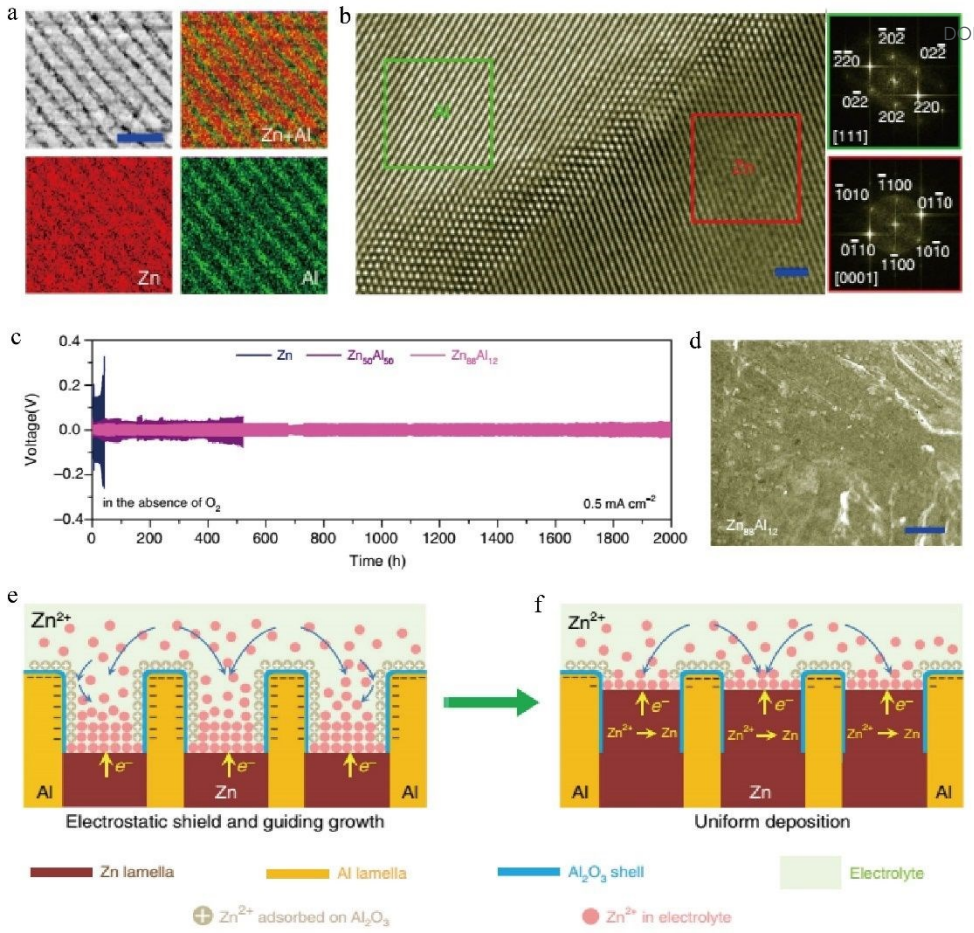

Fig.10 (a) EDS element mapping of Zn and Al in lamella-nanostructured eutectic $Zn_{88}Al_{12}$ alloys. Scale bar, 2 μm. (b) HRTEM image of Zn/Al interface of eutectic $Zn_{88}Al_{12}$ alloys (λ = ~450 nm). Scale bar, 1 nm, and FFT patterns of selected areas of HRTEM image that correspond to fcc Al and hcp Zn, respectively. (c) Long-term Zn stripping/plating cycling of symmetric batteries of monometallic Zn, hypoeutectic $Zn_{50}Al_{50}$ or eutectic $Zn_{88}Al_{12}$ alloys (λ = ~450 nm) at the current density of 0.5 mA cm^{-2} in aqueous $ZnSO_4$ electrolyte with the absence of O_2. (d) SEM images of eutectic $Zn_{88}Al_{12}$ (λ = ~450 nm), Scale bare, 5 μm. (e) Eutectic Zn/Al alloys with a lamellar structure composed of alternative Zn and Al nanolamellas in-situ produce core/shell interlayer patterns during the Zn stripping to guide the subsequent Zn plating. (f) The Al/Al_2O_3 interlayer patterns associated with insulative Al_2O_3 shield facilitate the uniform deposition of Zn. Reprinted with permission from ref. 101. Copyright 2020 Springer Nature.

View Article Online
DOI: 10.1039/D0EE02079F

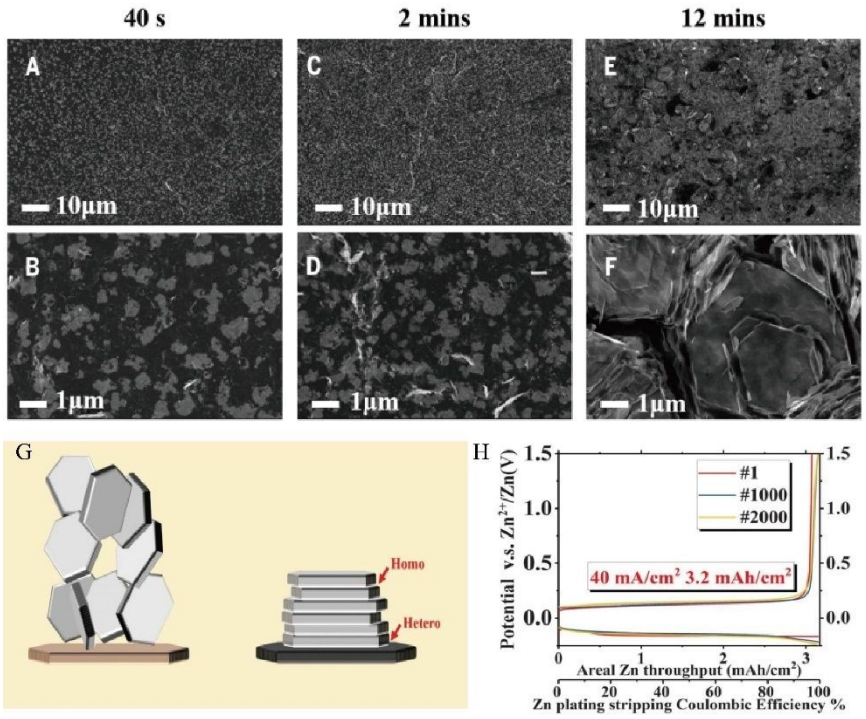

Fig.11 SEM of Zn deposits on graphene-coated stainless steel. SEM deposition times, (A and B) 40 s, (C and D) 2 min, and (E and F) 12 min. Current density, J = 4 mA/cm^2. (G) Scheme illustrating the design principle of epitaxial metal electrodeposition. (H) The voltage profile of epitaxial Zn metal anodes. Reprinted with permission from ref. 49. Copyright 2019 The American Association for the Advancement of Science.

View Article Online
DOI: 10.1039/D0EE02079F

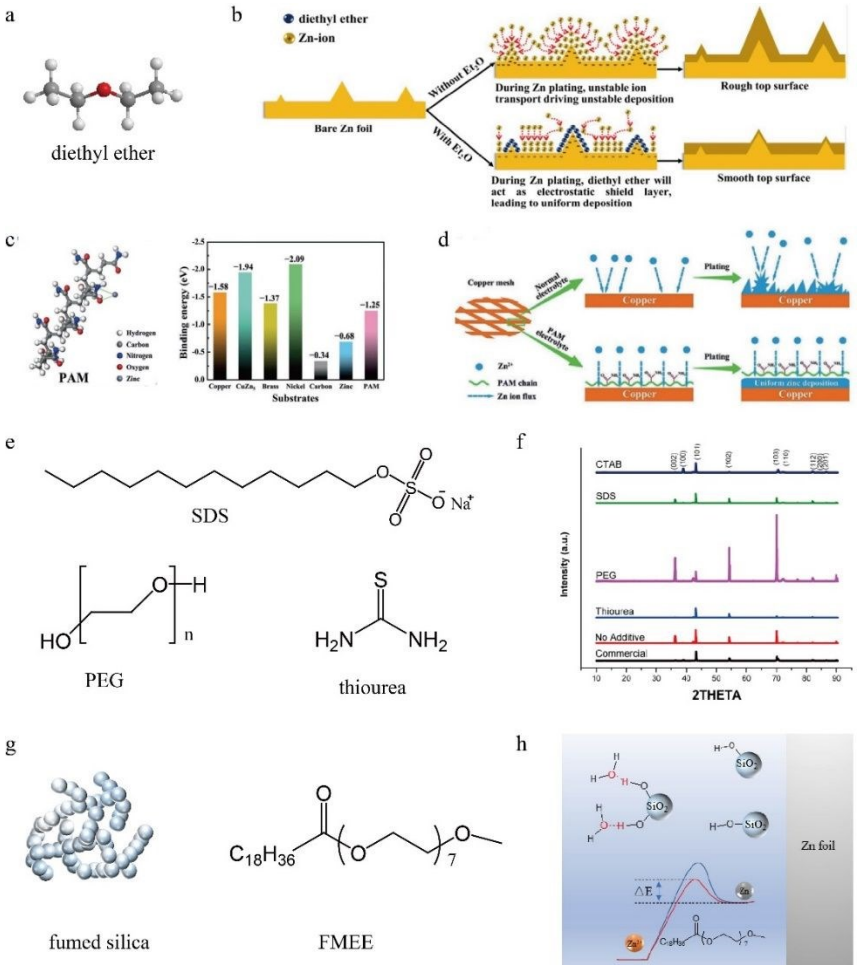

Fig.12 (a)molecular structure of Et_2O. (b) Schematics of morphology evolution for Zn anodes in mild aqueous electrolyte with and without Et_2O additive during Zn stripping/plating cycling. Reprinted with permission from ref. 104. Copyright 2019 Elsevier. (c) molecular structure of PAM and Binding energy of a zinc atom with different substrates. (d) Schematic illustration of zinc deposition on the copper mesh in normal and PAM added electrolytes. Reprinted with permission from ref. 105. Copyright 2019 Wiley-VCH Verlag GmbH & Co. KGaA, Weinheim. (e) molecular structures of SDS, PEG and Thiourea. (f) XRD results of the zinc anode electroplated with and without organic additives and commercialized zinc. Reprinted with permission from ref. 106. Copyright 2017 American Chemical Society. (g, h) molecular structures of fumed silica, FMEE, and corresponding mechanism for improving zinc anode processes.

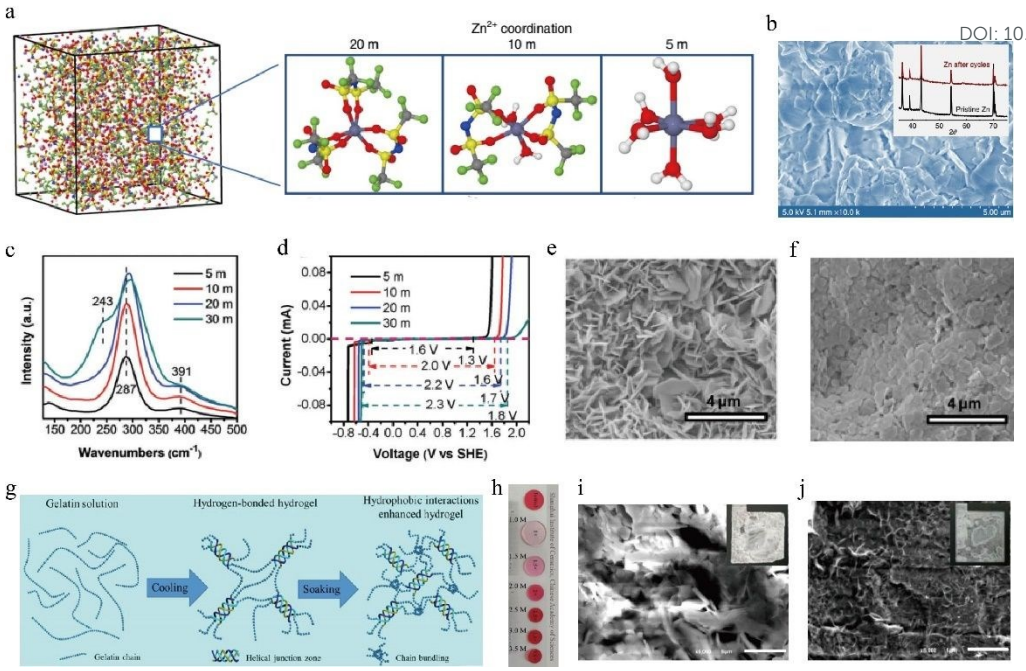

Fig.13 (a) Representative Zn^{2+}-solvation structures in the electrolytes with 1 m $Zn(TFSI)_2$ and three concentrations of LiTFSI (5 m, 10 m and 20 m) based on molecular dynamics (MD) simulations. (b) SEM image and XRD pattern (inset) of a Zn anode after 500 stripping/plating cycles in HCZE (1 m $Zn(TFSI)_2$ + 20 m liTFSI). Reprinted with permission from ref. 108. Copyright 2018 Springer Nature. (c) Raman spectra and (d) electrochemical stability window of the $ZnCl_2$ electrolyte at different concentrations. (e, f) SEM images of the Zn electrodes cycled for 75 times in beaker cells at 1 mA cm^{-2} with a sweep duration of 1 hour in 5 m and 30 m $ZnCl_2$. Reproduced from Ref. 110 with permission from The Royal Society of Chemistry. (g) The schematic illustration of molecular conformation of gelatin solution, gelatin solid-state electrolyte (GSE-0), and salt-reinforced GSE-x (x=1.0, 1.5, 2.0, 2.5, 3.0, and 3.5) after soaking the GSE-0 in $ZnSO_4/MnSO_4$ solution. (h) Optical images of GSE-x (x=1.0, 1.5, 2.0, 2.5, 3.0, and 3.5). (i, j) Optical and SEM images of Zn electrodes after cycling (400 cycles at current density of 5 mA cm^{-2}) in the Zn/Zn symmetric cells using GSE-0 and GSE-2.5 as solid-state electrolytes, respectively. Scale bar: 5 μm. Reproduced from Ref. 111 with permission from The Royal Society of Chemistry.

View Article Online
DOI: 10.1039/D0EE02079F

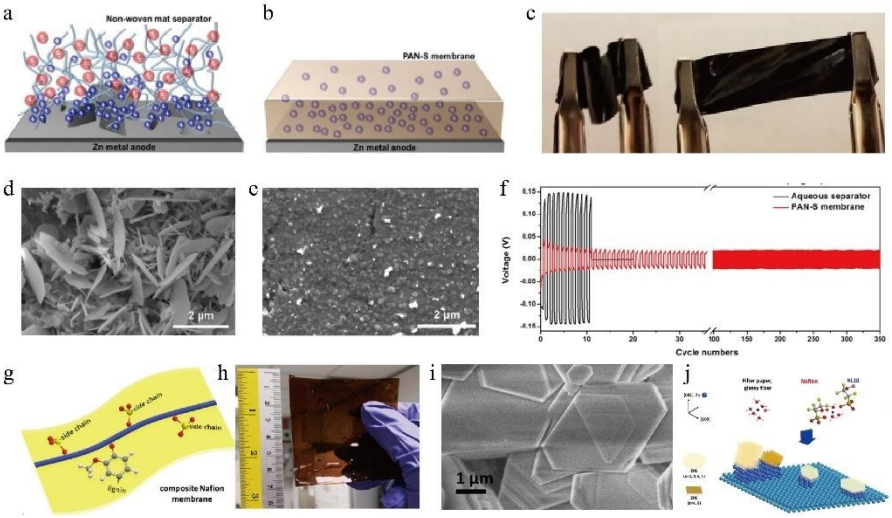

Fig.14 Schematic descriptions of Zn deposition: (a) Zn dendritic growth due to the ramified Zn deposition at the interface between the Zn metal and conventional separator and (b) dendrite growth suppression due to uniform Zn^{2+} concentration at the interface between the Zn metal and the single-ion transport membrane. (c) photographs of bent and stretched PAN-S film. SEM images of the Zn anode surface from the cells using a (d) aqueous separator and (e) PAN-S membrane. (f) Cycling performance comparison (Zn/Zn symmetric cell test at a current density of 0.5 mA cm^{-2}). Reprinted with permission from ref. 115. Copyright 2018 American Chemical Society. (g) Scheme illustrating the design of composite biomass waste lignin@Nafion membranes. (h) optical image of lignin@Nafion with a size of 7×7 cm^2. (i) Faceted lateral plates formed after the 1000th cycle. (j) Proposed scheme to summarize the effects of membranes on the surface of Zn metal. The interaction between $-SO_3^-$ from Nafion and Zn^{2+} may alter the Zn^{2+} coordination from its state in the electrolyte ($Zn^{2+}(H_2O)_6$). As a result, distinct growth modes of ZHS and deposited Zn are obtained. Reprinted with permission from ref. 116. Copyright 2019 Wiley-VCH Verlag GmbH & Co. KGaA, Weinheim.

View Article Online
DOI: 10.1039/D0EE02079F

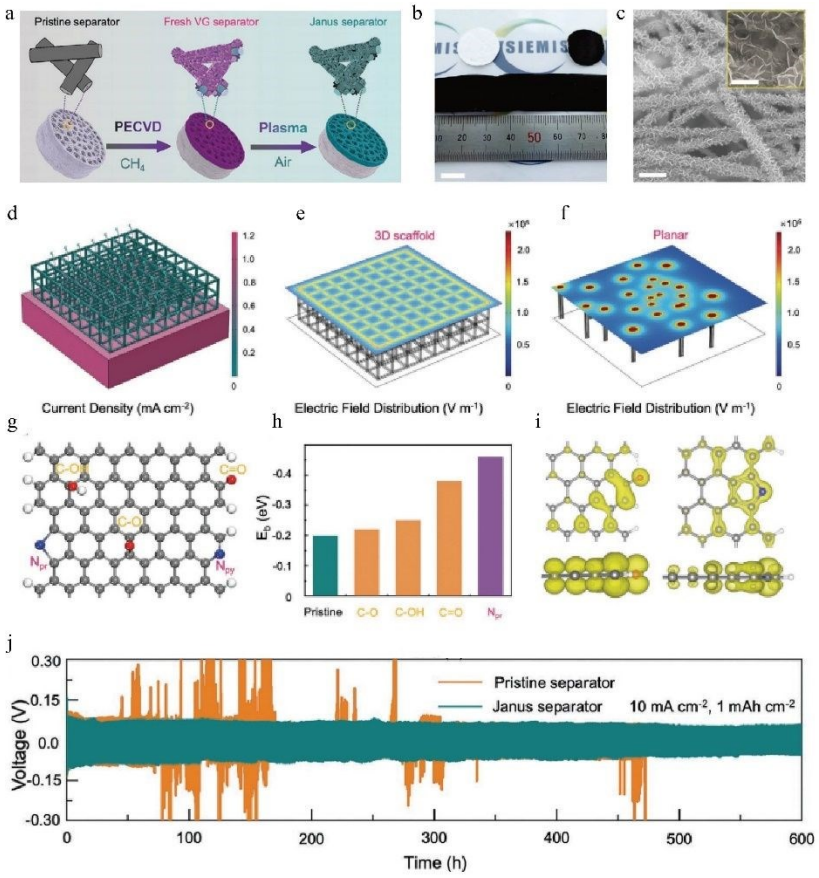

Fig. 15 a) Schematic representation of synthetic process of Janus separator. b) Digital photo of a VG carpet, pristine separator, and Janus separator. Scale bar: 1 cm. c) Top-view SEM image of VG carpet on the Janus separator. Scale bar: 1 μm. Inset: High-magnification SEM observation of VG. Scale bar: 100 nm. d) Current distribution in the 3D scaffold. Electric field distribution of e) 3D scaffold structure (Janus separator case) and f) 2D planar structure (pristine separator case). DFT simulation of Zn adsorption on O/N-functionalized graphene: g) Configuration of O and N-doped graphene. h) The binding energy of Zn atom on the O/N functionalized graphene. i) The yellow contour with the isosurface value of 0.002 e bohr^{-3} of partial charge density around the fermi level by top-view (upper) and side-view (lower) in the C=O-G and C-N_{pr}-G configuration from left to right. (j) Long-cycle voltage–time profiles at a current density of 10 mA cm^{-2} with a capacity of 1 mAh cm^{-2}. Reprinted with permission from ref. 117. Copyright 2020 Wiley-VCH Verlag GmbH & Co. KGaA, Weinheim.

View Article Online
DOI: 10.1039/D0EE02079F

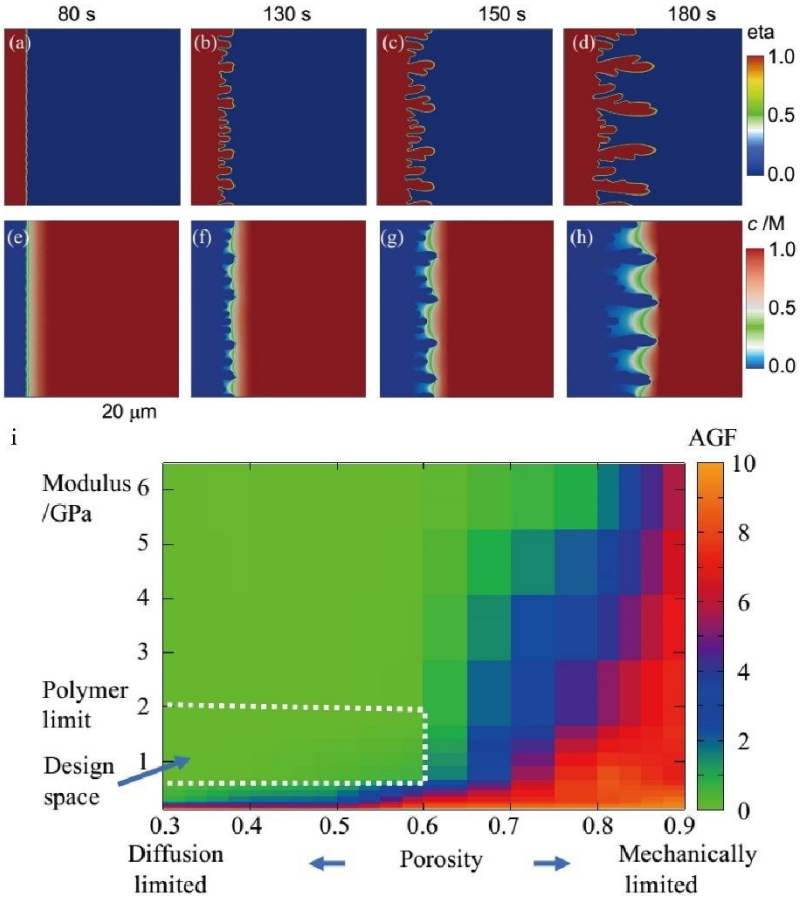

Fig.16 (a)-(d) Electrode Morphology evolution after Zn electrodeposition for 80 s, 130 s, 150 s and 180 s, respectively. (e)-(h) Corresponding Zn-ion concentration evolution. (i) Two-dimensional mapping of the AGF after electrodeposition of 120 s as a function of porosity and modulus, showing the practical design space that leads to dendrite suppression. Reprinted with permission from ref. 119. Copyright 2020 American Chemical Society.

View Article Online
DOI: 10.1039/D0EE02079F

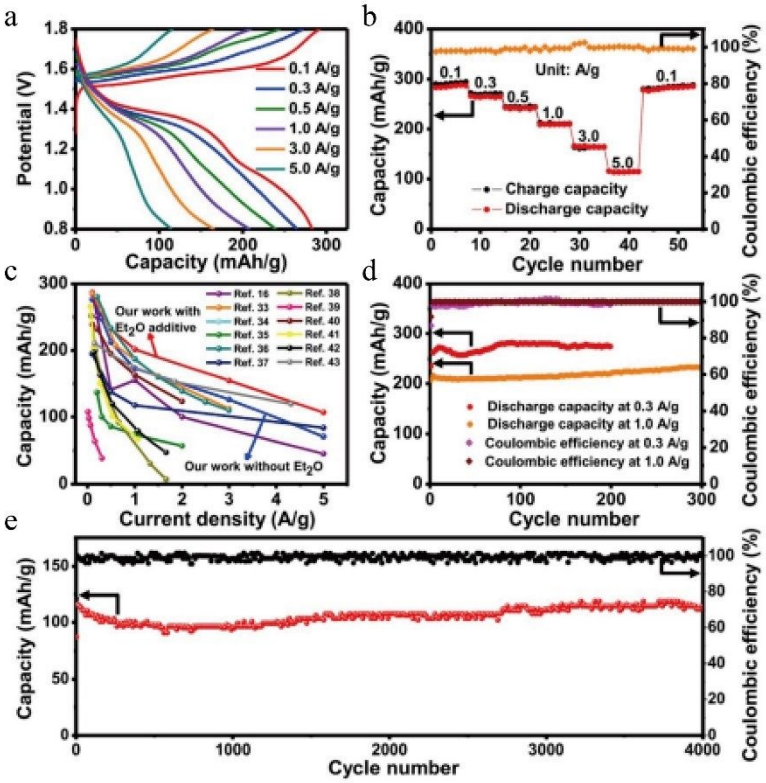

Fig.17 Cycling stability and rate capability of Zn–MnO_2 battery: (a) Galvanostatic charge-discharge curves of Zn–MnO_2 battery with 2 vol% Et_2O additives at different current densities. (b) The corresponding rate performance for Zn–MnO_2 battery with 2 vol% Et_2O additive. (c) Comparison of the rate capability of Zn–MnO_2 battery with other reported Mn-based ARZIBs in mild aqueous electrolyte. (d) Cycling performances of Zn–MnO_2 battery with Et_2O additive at 0.3 A/g and 1 A/g. (e) Long-term cycling performance of Zn–MnO_2 battery with Et_2O additive at 5 A/g. Reprinted with permission from ref. 104. Copyright 2019 Elsevier.

View Article Online
DOI: 10.1039/D0EE02079F

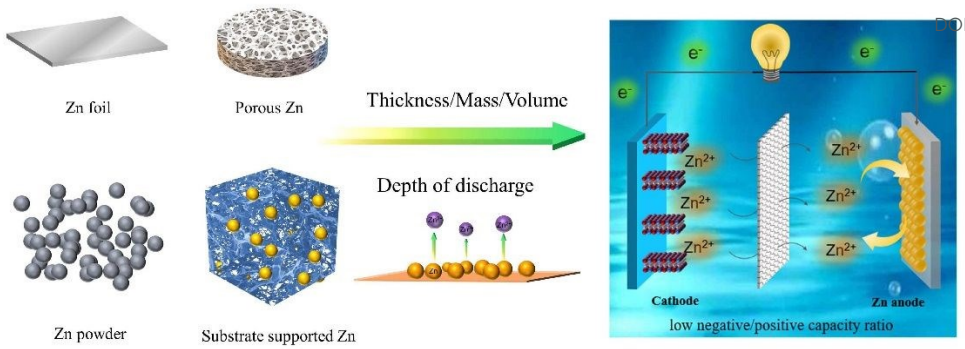

Fig.18 Several potential forms of zinc anode for constructing ZIBs with low negative/positive capacity ratio by minimizing the amount of zinc metal (optimizing thickness, mass and volume of zinc materials) and maximizing depth of discharge.

View Article Online
DOI: 10.1039/D0EE02079F

Table 1. Representative coating materials used for improving zinc anode and corresponding enhancement principles.

Coating materials		Enhancement principles	Ref.
Inorganic materials	Au nanoparticles	acting as hetero seeds	66
	ZrO_2 nanoparticles	1) homogenizing charge distribution of zinc anode surface via Maxwell-Wagner polarization 2) inert physical barrier for water/oxygen	68
Polymer	polyamide	1) regulating interfacial zinc ion diffusion behavior ; 2) inhibiting interfacial water/oxygen to suppress side reactions	82
Porous functional material	Kaolin	1) Homogenizing Zn^{2+} migration via selective channels 2) Suppressing HER and corrosion	75
	ZIF-7	Regulating solvation structure of zinc ions forming super-saturated electrolyte front surface	77
	Pyrolytic ZIF-8	Facilitating Zn^{2+} diffusion via channels and coordination interactions	76

View Article Online
DOI: 10.1039/D0EE02079F

Table 2. Summary of battery performances of zinc anode enhanced by various coating materials.

Coating materials	Preparation methods	Aqueous electrolyte/ separator	Cell performance	Ref.
Au nanoparticles (~100 nm)	ion beam sputtering of Au nanoparticles onto zinc foil	3 M $ZnSO_4$ / filter papers (Φ = 19 mm)	Cycling stability: **2000** h (0.25 mA cm^{-2}, 0.05 mAh cm^{-2}) Overpotential after initial activation: ~60 mV (vs. ~80 mV for bare Zn)	66
In microparticles (average 5 μm)	spontaneous galvanic replacement reaction between Zn metal and $InCl_3$	2.0 M $ZnSO_4$/ Two pieces of non-woven fabric membranes	Cycling stability: **1500** h (0.2 mA cm^{-2}, 0.2 mAh cm^{-2}) **500** h (1 mA cm^{-2}, 1 mAh cm^{-2}) Voltage hysteresis: 54 mV (vs. 261 mV for bare Zn under 0.2 mA cm^{-2} and 0.2 mAh cm^{-2})	67
ZrO_2 nanoparticles (average 35 nm)	Casting slurry of ZrO_2/PVDF/NMP onto zinc foil	2 M $ZnSO_4$ / glass fiber separator	Cycling stability: **3800** h (0.25 mA cm^{-2}, 0.125 mAh cm^{-2}), **2100** h (5 mA cm^{-2}, 1 mAh cm^{-2}) Initial CE: 95.5% (vs. 89.72% for bare Zn), nucleation overpotential: 55.2 mV (vs. 75.1 mV for bare Zn) under 5 mA cm^{-2} and 1 mAh cm^{-2})	68
Al_2O_3	atomic layer deposition (trimethylaluminum and H_2O) on zinc foil (0.2 mm in thickness)	3 M $Zn(SO_3CF_3)_2$ (200 μL)/fibers(separator, Φ = 5/8 inch)	Cycling stability: **500** h (1 mA cm^{-2}, 1 mAh cm^{-2}) Voltage hysteresis: 36.5 mV (vs. 73.7 mV for bare Zn)	70
three-dimensional nanoporous ZnO	in-situ $Zn(OH)_4^{2-}$ deposition onto zinc foil (0.1 mm thickness)	2 M $ZnSO_4$ + 0.1 M $MnSO_4$/glass fiber separators (Φ = 19 mm, Whatman)	Cycling stability: **500** h (5 mA cm^{-2}, 1.25 mAh cm^{-2}) nucleation overpotential: 42.4 mV (vs. 66.9 mV for bare Zn) at 1 mA cm^{-2} CE: average 99.55% (at 2 mA cm^{-2})	71
ZIF-8 and its pyrolysis products	in-situ growth of ZIF-8 onto Zn foil (250 μm thick)	2 M $ZnSO_4$/ Whatman glass fiber filter	Cycling stability: **400** h (1 mA cm^{-2}, 1 mAh cm^{-2}), **400** h (10 mA cm^{-2}, 10 mAh cm^{-2}) Overpotential: 52.5 mV for ZIF-8/Zn, 91.5 mV for C-650/Zn at 5 mA cm^{-2}	76
ZIF-7	Blade casting slurry of ZIF 7/PVDF/DMF onto Zn foil (thickness: 20 μm)	2 M $ZnSO_4$ (50 μL)/ Glass fiber	Cycling stability: **3000** h (0.5 mA cm^{-2}, 0.5 mAh cm^{-2}) Overpotential: 28 mV at 0.3 mA cm^{-2}.	77

Kaolin	Scrape coating slurry of Kaolin/PVDF/NMP onto zinc foil (Φ = 15 mm, δ= 0.1 mm)	2 M $ZnSO_4$ + 0.1 M $MnSO_4$/glass fiber separators (Φ = 19 mm, Whatman)	Cycling stability: **800** h, Voltage hysteresis: ≈0.07 V (4.4 mA cm^{-2}, 1.1 mAh cm^{-2}) Nucleation overpotential: 41.3 mV (vs. 80.6 mV for bare Zn) at 2 mA cm^{-2}	75
Nanoporous CaCO3	Casting slurry of $CaCO_3$/PVDF/NMP onto zinc foil	3 M $ZnSO_4$ + 0.1 M $MnSO_4$/ glass fiber separator	Cycling stability: **836** h. Voltage hysteresis: 80 mV (vs. 230 mV for bare Zn) (0.25 mA cm^{-2}, 0.05 mAh cm^{-2})	74
Hydrogen-substituted graphdiyne (HsGDY)	in-situ growth of HsGDY onto Zn plate	2 M $ZnSO_4$/ Nonwoven fiber film	Cycling stability: **2400** h, Voltage hysteresis: 62-120 mV (vs. 164-228 mV for bare Zn) (0.5-2 mA cm^{-2}, 0.1 mAh cm^{-2}),	81
carbon black+ nanofibrillated cellulose (NFC)	drop casting slurry of carbon black and NFC	2 M $ZnSO_4$ + 0.2 M $MnSO_4$/Whatman GF/A filter paper	Cycling stability: **400** h, (5 mA cm^{-2}, 5 mAh cm^{-2}), Voltage hysteresis: 160 mV (vs. 280 mV for bare Zn) at 0.5 mA cm^{-2}.	80
Polyamide (PA)@ $Zn(TfO)_2$	Blade casting solution of PA and $Zn(TfO)_2$ onto zinc plate/foil	2 M $ZnSO_4$ / glass fiber separator	Cycling stability: **8000** h Polarization voltage: ~0.1V (0.5 mA cm^{-2}, 0.25 mAh cm^{-2}) CE: average 95.12% (0.4 mA cm^{-2}, 0.4 mAh cm^{-2})	82
Polyvinyl butyral (PVB)	Spin coating PVB/ethanol solution onto zinc foil (0.01 mm)	1 M $ZnSO_4$/	Cycling stability: **2200** h (0.5 mA cm^{-2}, 0.5 mAh cm^{-2}), Polarization voltage: 108.5 mV (vs. 200 mV for bare Zn) CE: average 99.4% (vs. 93.8% for bare Zn)	83
PVDF@ TiO_2	drop casting slurry of PVDF and nanosized TiO_2 onto Zn foil	2 M $ZnSO_4$ (100 μL)/ Glass fiber separator (Φ19)	Cycling stability: **2000** h (0.885 mA cm^{-2}, 0.885 mAh cm^{-2}), **250** h (8.85 mA cm^{-2}, 8.85 mAh cm^{-2}) CE: average 99.4% after the initial three activation cycles polarization voltage: 71.2 mV for 150th, 50.1 mV for 350th (1.77 mA cm^{-2}, 0.885 mAh cm^{-2})	84
Nafion-Zn-X	evaporating solution of Nafion and Zn-X in rectangular Zn (300 μm) groove	2 M $ZnSO_4$ (80 μL)/ dust-free paper (55% cellulose + 45% polyester)	Cycling stability: **1000** h (1 mA cm^{-2}, 10 mAh cm^{-2}), CE: 97% after initial several cycles at 0.2 mA cm^{-2}. Polarization voltage: 50 mV (vs. 90 mV for bare Zn at 2 mA cm^{-2}.	85

Note: CE: Columbic efficiencies of zinc stripping/plating based on asymmetric half-cells.

View Article Online
DOI: 10.1039/D0EE02079F

Table 3. Summary of battery performances of zinc anode enhanced by internal structure optimization.

Zinc electrode structures	Preparation methods	Aqueous electrolyte/ separator	Cell performance	Ref.
3D nanoporous Zn metal electrode	Electrochemical/thermal treatment of zinc foil	2 M $Zn(CF_3SO_3)_2$ / glass fiber separator	Cycling stability: **1400** h (0.5 mA cm^{-2}, 0.1 mAh cm^{-2}), **200** h (5 mA cm^{-2}, 10 mAh cm^{-2}) Overpotential: ~ 60 mV (vs. 200 mV for bare Zn) at 0.5 mA cm^{-2}. ~ 250 mV (vs. 1200 mV for bare Zn) at 10 mA cm^{-2}.	86
Multifunctional CNT framework hosted zinc anode	electrodeposition method (0.5 M $ZnSO_4 \cdot 7H_2O$, 1 M Na_2SO_4, and 0.3 M H_3BO_3)	2 M $ZnSO_4$ (200 µL)/ glass fiber separator	Cycling stability: **200** h (2 mA cm^{-2}, 2 mAh cm^{-2}), **110** h (5 mA cm^{-2}, 2.5 mAh cm^{-2}) CE: 97.9% after first two cycles. Voltage hysteresis: 27 mV (2 mA cm^{-2}), 68 mV (5 mA cm^{-2}) Nucleation overpotential: 84 mV (vs. 192 mV for bare Zn) at 5 mA cm^{-2}.	90
Conductive graphite fiber hosted zinc anode	electrodeposition method (6 mA h cm^{-2} of zinc)	0.5 M Na_2SO_4 and 0.05 M $ZnSO_4$/ glass fiber separator	Cycling stability: **700** h Voltage hysteresis: around 50 mV (1 mA cm^{-2}).	88
$Ti_3C_2T_x$ MXene@Zn Paper	Electrochemical deposition approach (4 mAh cm^{-2} of metallic Zn was electroplated at 1 mA cm^{-2})	2 M $ZnSO_4$/ Glass microfiber (Whatman)	Cycling stability: **300** h. Voltage hysteresis: 75 mV (vs. 109 mV for bare Zn). CE: average 94.13% (1 mA cm^{-2}, 1 mAh cm^{-2})	96
Porous copper foam hosted zinc anode	Electrochemical deposition approach (3 mA cm^{-2} with a discharge capacity of 3.39 mA h)	2 M $ZnSO_4$/ glass microfiber membrane (Whatman)	Cycling stability: **300** h (2 mA cm^{-2}, 1 mAh cm^{-2}) Nucleation overpotential**:** 65.2 mV (3 mA cm^{-2}, 3 mAh cm^{-2}). CE: close to 100%	97
Zn/stainless steel mesh composite	embedding Zn foil in 304 stainless steel mesh via calendaring	3 M $Zn(SO_3CF_3)_2$ /	Cycling stability: **300** h (2 mA cm^{-2}, 1 mAh cm^{-2})	99
Lamella-nanostructured eutectic zinc–aluminum alloys	Metallurgical technology	2 M $ZnSO_4$ (O_2-absent)/ glass fiber membrane	Cycling stability: **2000** h. Overpotential: ~ 20 mV (vs. 101 mV for bare Zn) at 0.5 mA cm^{-2}.	101
Cu-Zn nanoalloy/Zn anode	replacement reaction and electrochemical conversion	3 M $ZnSO_4$/ glass fiber separator	Cycling stability: **1500** h. Overpotential: 46 mV (vs. > 400 mV for bare Zn) (1 mA cm^{-2}, 0.5 mAh cm^{-2})	103

View Article Online
DOI: 10.1039/D0EE02079F

Table 4. Summary of battery performances of zinc anode enhanced by electrolyte optimization.

Electrolyte optimization methods	Cell performance	Ref.
Diethyl ether as self-healing electrolyte additive	Cycling stability: **250** h. Voltage hysteresis: 44 mV (vs. 96 mV for normal electrolyte). (0.2 mA cm^{-2}, 0.2 mAh cm^{-2})	104
Zinc-oriented polyacrylamide electrolyte additive	Cycling stability: **180** h (1 mA cm^{-2}, 1 mAh cm^{-2}), **280** h (2 mA cm^{-2}, 4 mAh cm^{-2}), **350** h (0.2 mA cm^{-2}, 1 mAh cm^{-2}) CE: near 100% at 20 mA cm^{-2}. Voltage hysteresis: 93.1 mV (vs. 127.1 mV for normal electrolyte) at 2 mA cm^{-2}, 4 mAh cm^{-2}.	105
$ZnSO_4$+fumed silica+fatty methyl ester ethoxylate electrolyte	Cycling stability: **1500** h. Voltage hysteresis: 91 mV (vs. 121 mV for normal electrolyte) (0.2 mA cm^{-2}, 0.2 mAh cm^{-2})	107
An aqueous electrolyte based on Zn and lithium salts at high concentrations (1 m $Zn(TFSI)_2$ + 20 m LiTFSI)	Cycling stability: **170** h (0.2 mA cm^{-2}) CE: approaching 100% after the second cycle	108
A $ZnCl_2$ water-in-salt electrolyte	Cycling stability: **600** h (0.2 mA cm^{-2}) CE: 95.4% (1 mA cm^{-2})	110
Inorganic salt reinforced Zn^{2+}-conducting solid-state electrolyte	**400** h (5 mA cm^{-2}, 2.5 mAh cm^{-2})	111
$Zn(ClO_4)_2$ electrolyte	Cycling stability: **3500** h (0.5 mA cm^{-2}, 0.5 mAh cm^{-2}), **3000** h (1 mA cm^{-2}, 1 mAh cm^{-2}) CE: average 99.3% (2 mA cm^{-2})	112